Lithos 396–397 (2021) 106192

Contents lists available at ScienceDirect

Lithos

journal homepage: www.elsevier.com/locate/lithos

Research Article

Petrogenesis of primitive lavas from the Toro Ankole and Virunga Volcanic Provinces: Metasomatic mineralogy beneath East Africa's Western Rift

Erica Pitcavage [a,d,*], Tanya Furman [a], Wendy R. Nelson [b], Peggy K. Kalegga [c], Erasmus Barifaijo [c]

[a] Dept. of Geosciences, Pennsylvania State University, University Park, PA 16802, USA
[b] Dept. of Physics, Astronomy, and Geosciences, Towson University, Towson, MD 21252, USA
[c] Dept. of Geology and Petroleum Studies, Makerere University, Kampala, Uganda
[d] Dept. of Earth and Atmospheric Sciences, University of Houston, Houston, TX 77204, USA

ARTICLE INFO

Article history:
Received 10 December 2020
Received in revised form 11 April 2021
Accepted 24 April 2021
Available online 28 April 2021

Keywords:
East african rift
Metasomatism
Alkaline volcanism
Lithospheric melting

ABSTRACT

Geochemical analysis of magmas erupted in continental rifts are a valuable tool for understanding the compositional, physical, and thermal controls on rift related magmatism. Bulk rock geochemistry and geochronology of lavas from volcanic fields in the Western Rift of the East African Rift System provide insight into the sources and processes of petrogenesis of magmas in the region, as well as insight into the spatial variability of metasomatic history of the lithospheric mantle. Lava compositions from three primitive volcanic fields in southwestern Uganda (Bufumbira, Virunga Volcanic Province; Katwe-Kikorongo and Bunyaruguru, Toro Ankole Volcanic Province) are potassic ($K_2O/Na_2O = 0.3–2.7$) and enriched in incompatible trace elements (e.g., $(La/Yb)_n = 12–132$); the Toro Ankole samples are also silica-undersaturated. The compositions of these lavas require significant input from metasomatized sub-continental lithospheric mantle (SCLM), likely consisting of a pyroxenite containing variable amounts of garnet, amphibole, phlogopite, and accessory minerals including titanite, apatite, and zircon, produced through infiltration by spatially varying carbonatitic and silicate metasomatic agents. A subset of lavas record $^{40}Ar/^{39}Ar$ ages = 21–662 ka, with minor geographic and compositional trends apparent in the temporal development of the volcanic fields.

1. Introduction

The geochemical composition of continental basaltic magmas is an extremely important tool in understanding processes related to the formation, evolution, and stability of continents and the associated subcontinental lithospheric mantle (SCLM). Temporal and spatial variability in the geochemistry of basalts derived from the SCLM can document the compositional variability of the lithosphere and its evolution through time. Primitive magma compositions also provide insight into the depth and extent of melting, which enhances our understanding of physical processes responsible for magma generation and continental evolution—results of the continental rifting process. Continental rifting combines melts of SCLM, ambient asthenospheric mantle and, if present, mantle plume material to produce basaltic volcanism, the composition of which can be utilized to unravel the nature of mantle material and melting processes responsible for its production.

The East African Rift System (EARS) provides an important opportunity to study process variables across lithosphere of differing ages, thicknesses and compositions through characterizing the diversity in the timing, composition, and volumes of rift-related magmatism. The Western Rift of the EARS is characterized by volumetrically less significant volcanism than the Main Ethiopian Rift (MER) and the Eastern Rift, and substantial portions of the Western Rift are amagmatic. Subsurface indicators of magmatic activity also differ between regions of the EARS: studies using seismic tomography have found evidence for broadly distributed low-velocity zones beneath much of the Eastern Rift and MER, while low velocity areas appear localized within the lithosphere under Western Rift volcanic provinces (Emry et al., 2018).

Here we explore the magma source characteristics for primitive melts from the Toro Ankole and Virunga volcanic provinces in the northern portion of the EARS Western Rift. We use the compositions of primitive basalts from monogenetic cinder cone fields in each province as a tool to understand mantle source mineralogy, metasomatic history, and melting depth and extent: relative to more evolved magmatic systems found elsewhere in Virunga (Chakrabarti et al., 2009a; Rogers et al., 1998, 1992), these primitive lava compositions provide a more direct link to primary melt characteristics. High-precision

* Corresponding author at: Dept. of Geosciences, Pennsylvania State University, University Park, PA 16802, USA
E-mail address: epitcava@central.uh.edu (E. Pitcavage).

https://doi.org/10.1016/j.lithos.2021.106192
0024-4937/

$^{40}Ar/^{39}Ar$ geochronology of these volcanic products was used to assess variability in melting and transport processes over time and determine the evolution of the magmatic plumbing systems. The results of this study provide insight into the along-axis evolution of lithospheric properties relevant to rift-related magmatism, and further constrain the complex tectonic and geochemical evolution of the lithospheric mantle in East Africa.

2. Geologic background

The East African Rift System is Earth's largest modern manifestation of continental rifting. Extensive rift-related magmatism began in the Oligocene (~30 Ma) in association with the Afar mantle plume, producing voluminous tholeiitic basalt magmatism in the Afar region, though the earliest volcanic activity recorded in the rift system occurred in the Eocene in Turkana, Kenya and southern Ethiopia at approximately 45 Ma. This was followed by pulses of voluminous basaltic volcanism in the Oligocene and early Miocene (Baker et al., 1996; Ebinger et al., 2000, 1993; George et al., 1998; Pik et al., 1998; Rooney, 2017; Stewart and Rogers, 1996). Breakup of the Afro-Arabian shield produced a triple junction with arms forming the Red Sea, the Gulf of Aden and the EARS. Further rifting and magmatism followed to the south, forming the Main Ethiopian Rift (MER), and the Eastern Rift of the EARS, sometimes referred to as the Kenya (or Gregory) Rift and the Western (or Albertine) Rift (Chorowicz, 2005). Post-Miocene to Recent magmatic activity in the Eastern Rift and MER is dominantly alkaline. Additionally, minor carbonatite lavas are found along rift margins and in isolated volcanic edifices in both Kenya and Tanzania (Woolley and Church, 2005).

The EARS Western Rift has hosted less volumetrically extensive magmatism than the MER or Eastern Rift. Western Rift volcanism is restricted to four discrete volcanic provinces—Rungwe, Kivu, Virunga, and Toro Ankole—located in accommodation zones separating amagmatic rift basins (Ebinger, 1989; Fig. 1). The tectono-magmatic zone defined by the Western Rift is separated from the Eastern Rift by the rigid Archean Tanzanian craton. Kinematically, the Tanzanian Craton behaves as the largely independent Victoria Microplate (Stamps et al., 2008), which moves eastward relative to central Africa at velocities less than those of the Rovuma and Somalian microplates east of the Eastern Rift (Fig. 1a). Like many other portions of the EARS, the Western Rift follows zones of pre-existing lithospheric weakness: mobile belts formed by late Neoproterozoic Pan-African Orogeny tectonic events (Begg et al., 2009). Timing of the development of Western Rift fault structures is debated (e.g. Roberts et al., 2012) but appears to have been underway by ~12 Ma when the earliest volcanic products erupted in NW Virunga and Kivu (Kampunzu et al., 1998; Pouclet et al., 2016).

We focus here on young (<600 ka) primitive lavas from volcanic fields in the Virunga and Toro Ankole provinces (Fig. 1). Previous work in the region has identified lithospheric mantle material as an important source region for the Western Rift magmas, which are compositionally diverse and are dominated by highly alkaline erupted products and occasional carbonatites (Boven et al., 1998; Furman and Graham, 1999; Lloyd, 1981; Muravyeva and Senin, 2016; Rogers et al., 1998; Rosenthal et al., 2009), though Chakrabarti et al. (2009a) proposed a heterogeneous mantle plume source to explain compositional variability in the Western Rift. Toro Ankole, located in southwestern Uganda, is the northernmost and structurally youngest volcanic province of the Western Rift; it contains four volcanic fields: Fort Portal, Ndale, Bunyaruguru and Katwe-Kikorongo. Samples discussed here are from volcanoes in Katwe-Kikorongo and Bunyaruguru (Fig. 1b). Volcanism in Toro Ankole has largely consisted of explosive, volatile-rich eruptions characterized by small maars, craters, and tuff deposits, with minor lava flows and volcanic bombs (Holmes and Harwood, 1932), all previously dated ≤450 ka, primarily <80 ka (Boven et al., 1998; Kampunzu et al., 1998) with K-Ar and Ar-Ar. Toro Ankole lavas contain a wide range of metasomatized mantle xenoliths, some of which have been described in detail previously (e.g. Davies and Lloyd, 1989; Lloyd, 1981; Lloyd et al., 1985; Muravyeva and Senin, 2018) and which help us characterize the underlying SCLM.

The Virunga Volcanic Province spans portions of Uganda, Rwanda, and the Democratic Republic of the Congo (Fig. 1c). It contains eight shield and stratovolcanoes, including currently active Nyamuragira and Nyiragongo; the latter has erupted undersaturated feldspathoid-bearing lavas (Figs. 1 & 2). Sabinyo and Karisimbi volcanoes erupted both mafic and evolved lavas (mugearites, benmoreites and trachytes) which have been interpreted variously as the result of divergent magma evolution trends (leucite basanite and leucite-melilite nephelnite; Pouclet et al., 2016), as products of crustal contamination (De Mulder et al., 1986; Rogers et al., 1998), and as melts of metasomatized lithosphere (e.g. Vollmer and Norry, 1983). Three cinder cone fields located adjacent to central volcanoes in Virunga have produced primitive alkaline mafic lavas: (1) the Bufumbira volcanic field, which is the focus of this study (2) Karisimbi primitive K-basanites (PKBs; Rogers et al., 1992) and (3) cinder cones located between Sabinyo and Visoke (Rogers et al., 1998). The Bufumbira volcanic field is located slightly outside the rift axis, east of the border fault bounding the eastern edge of the Rutshuru basin (Ebinger, 1989) and forms the northeastern extent of the Virunga province. Crustal faults in this area are dominantly NNW-SSE and frequently align with cone/vent locations (Pouclet et al., 2016). Lavas from the Virunga Province have been dated to ages up to 12 Ma (Kampunzu et al., 1998), though the major edifices present in the province are dominated by lava flows <300 ka (Chakrabarti et al., 2009b; De Mulder and Pasteels, 1986; Kampunzu et al., 1998; Rogers et al., 1998).

Primitive Bufumbira lavas are strikingly similar in major and trace element and isotopic composition to the Karisimbi PKBs (Rogers et al., 1992). Unlike more evolved lavas erupted from Karisimbi's main edifice, the PKB suite erupted from adventive cones on the southern flanks of Karisimbi volcano. They represent a primitive endmember for Karisimbi volcanics and are derived from an enriched (metasomatized) lithospheric mantle source. The PKBs and the Bufumbira cones are morphologically similar, display analogous geochemical signatures and overlap in age (primarily <100 ka). For these reasons, we explore some aspects of their petrogenesis together.

3. Methods

Rock samples with BU- and KK- identification numbers were cut to remove weathered portions and polished to remove potential contamination from saw marks. Polished pieces were chipped in a ceramic jaw chipper and powdered in an alumina ceramic shatterbox. Major element analysis was performed on a lithium metaborate fusion preparation of the powdered samples and measured using a Perkin-Elmer Optima 5300DV ICP-AES instrument at Penn State University calibrated with USGS rock standard BHVO-1. For trace element analysis, powdered samples were dissolved in an acid digestion procedure similar to Johnson and Plank (2000) and Kelley et al. (2003). Samples were first dissolved using a mixture of hydrofluoric and nitric acid, followed by hydrochloric acid and then nitric acid, with solutions dried down between each dissolution step. Samples were ultimately dissolved in a solution of 2% nitric acid and analyzed using a Thermo X-Series II quadrupole ICP-MS at the Pennsylvania State University using an internal standard of indium. USGS rock standards BHVO-1, BCR-1, BIR-1, JA-1, PCC-1 and W-2 were prepared using the same procedure and used to create calibration curves for each trace element (Supplementary information). This study includes new and previously unpublished analyses of several samples from the classic Combe collection, obtained from Western Rift volcanic provinces in the 1920s–1940s by Arthur Combe of the Geological Survey of Uganda (Holmes and Harwood, 1937, 1932). The major and trace element analyses of the Combe samples (C-prefix) were collected as described in Furman (1995).

Sample preparation and analysis for $^{40}Ar/^{39}Ar$ dating were performed in the Argon Geochronology Laboratory at Oregon State

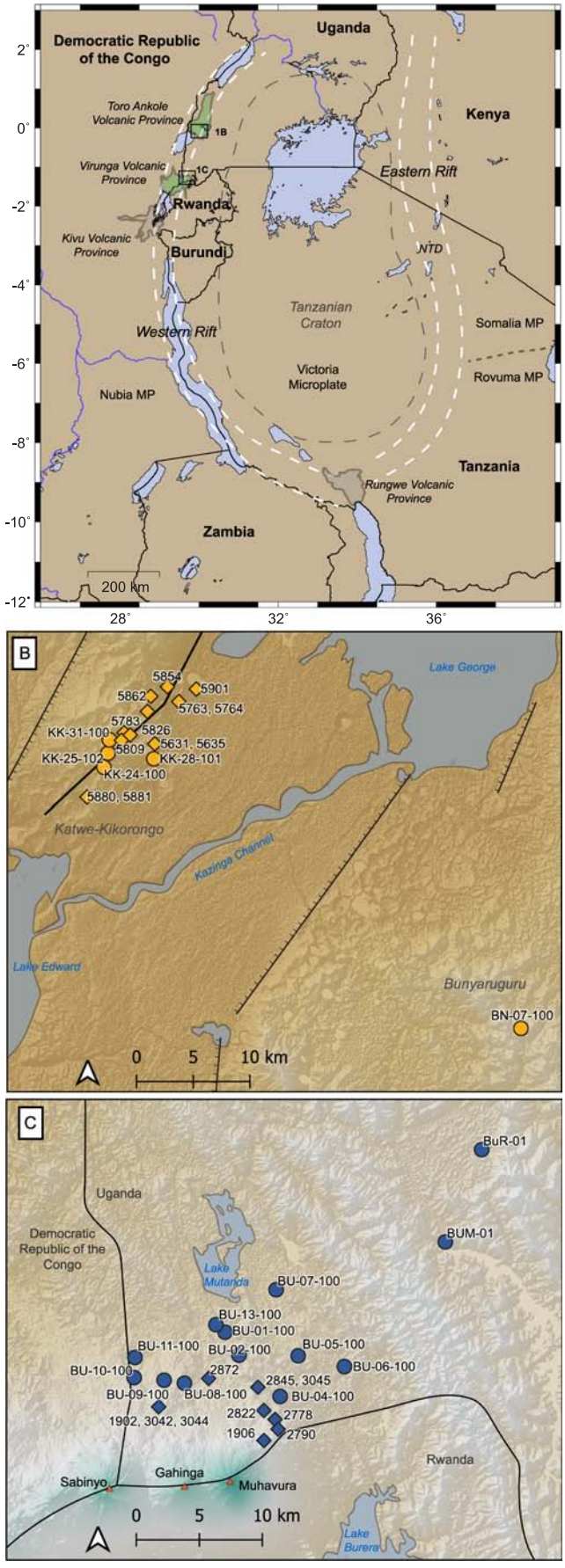

University generally following methods described in Konrad et al. (2019) and Koppers et al. (2000). Groundmass separates were dated for 13 lavas from Toro Ankole and Bufumbira; separates of phlogopite (BU-09-100) and plagioclase feldspar (BU-11-100) were also dated. In brief, whole rock samples were crushed with a jaw crusher and sieved to multiple size fractions, then rinsed in deionized water in an ultrasonic bath. Separation of phases was performed using a Frantz magnetic separator (current 0.1–0.7 amps). Samples were then leached multiple times in hydrochloric acid (1 N, 6 N) followed by nitric acid (1N, 3N) to remove alteration phases; feldspar separates were additionally leached in hydrofluoric acid. Relatively phenocryst-poor, alteration-free chips were picked from the desired size fraction—dominantly 150–250 μm but varied for some samples (Table 2). Samples and flux monitors were irradiated in the Oregon State TRIGA Reactor for 6 h. Argon isotopic ratios were measured using an ARGUS-VI mass spectrometer with the flux monitor standard Fish Canyon Sanidine (FCT-NM); results were calculated based on a standard age of 28.201 ± 0.023 Ma for FCT-NM (Kuiper et al., 2008) using the decay constant and age equations of Min et al. (2000). All samples were measured with incremental step laser heating; phlogopite separates from BU-09-100 were also measured with total fusion by single crystal laser heating. Data were reduced using the ArArCalc software (Koppers, 2002).

4. Results

4.1. Petrography

The Bufumbira lavas display a broad range of heterogeneous petrographic features. Some lavas are very poorly crystalline (BU-09-100, BU-13-100), some have >50% phenocrysts (BU-04-101, BU-05-100, BU-06-100), and some are highly vesicular with moderate (~30–40%) crystallinity (e.g., BU-01-100, BU-04-100, BU-08-100). Most lavas contain varying proportions of olivine and clinopyroxene. These minerals showed textural variations from homogenous euhedral to subhedral grains to zoned and/or resorbed grains which may be xenocrystic. Crystal clusters are often but not exclusively composed of clinopyroxene; the grains within the clusters are rounded, suggesting that these are xenocrystic and/or cumulate clusters which have undergone rounding prior to incorporation into the erupted lavas (e.g. BU-01-00, BU-06-100, BU-10-100). Some of the more evolved samples contain notable amounts of feldspar (dominantly plagioclase) as phenocrysts (BU-11-100) and/or groundmass phases (BU-08-100, BU-09-100, BU-10-100).

The Toro Ankole (Katwe-Kikorongo and Bunyaruguru) lavas have a variety of textures and include extremely crystal-poor (KK-24-100) and crystal-rich (KK-28-101, KK-31-100) lavas. Katwe-Kikorongo samples are olivine-poor and dominated by pyroxene, while the Bunyaruguru sample contains ~20% olivine.

Clinopyroxene from both volcanic fields is primarily diopside with Mg# 64-90, measured with a Cameca SX5 electron microprobe. Olivine has compositions of $Fo_{66\text{-}91}$ (Bufumbira) and $Fo_{73\text{-}86}$ (Katwe-Kikorongo); Mg content of olivine generally correlates with bulk composition in Bufumbira. Additional mineral composition data will be discussed in a future contribution; representative mineral compositions utilized in fractionation calculations are listed in Table 3. The Combe samples were analyzed geochemically with available bulk rock

Fig. 1. A) Map of Western Rift volcanic provinces, Tanzanian Craton, and major structures of the Western and Eastern Rifts of the EARS. Microplate names and locations from Stamps et al. (2008). Western Rift volcanic province (VP) areas after Barker and Nixon (1989), Furman (1995), Pouclet et al. (2016). NTD = Northern Tanzania Divergence. B) sample locations for Katwe-Kikorongo samples; C) sample locations for Bufumbira samples; diamonds indicate Combe collection samples (Holmes and Harwood, 1932, 1937); circles indicate samples collected by the authors. Data sources and mapping tools: (MacGregor, 2015); Wessel et al., 2019); NASA SRTM). Map produced using QGIS and GMT software.

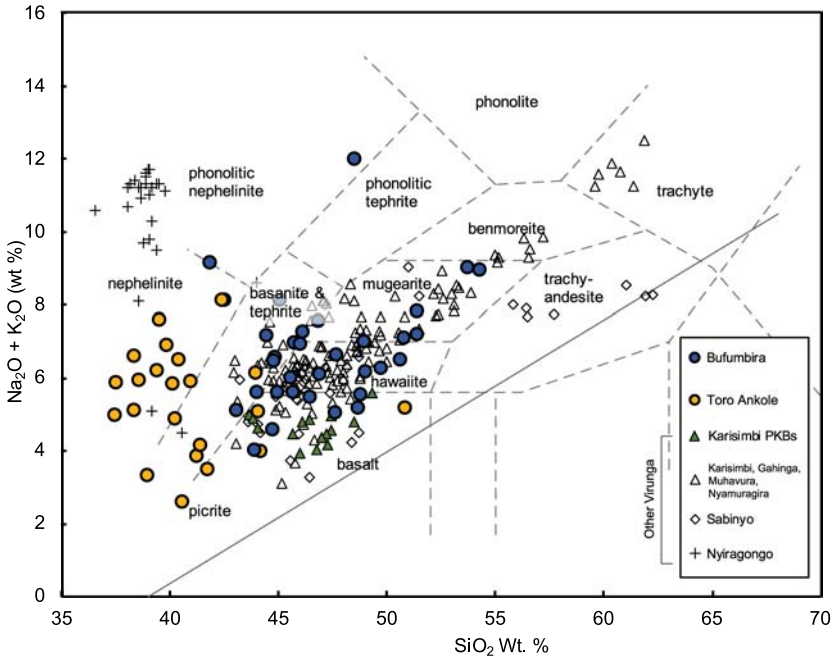

Fig. 2. Total alkali vs silica diagram (after Cox, 1979) for Toro Ankole and Bufumbira samples, with lavas from other Virunga volcanoes (Rogers et al., 1992, 1998; (Aoki et al., 1985), Chakrabarti et al., 2009a, 2009b) for comparison. Karisimbi, Gahinga, and Muhavura overlap with Bufumbira lavas at lower values of SiO_2, but extend to more evolved compositions along the basalt-hawaiite-mugeartie-benmoreite-trachyte series. Lavas from Sabinyo and nearby cones follow a similar but less alkalic trend. Nyiragongo, an active edifice in the Democratic Republic of the Congo, erupts silica-undersaturated and commonly phonolitic or nephelinitic compositions.

powders; thin sections were not available for assessment, though most of these samples have been described previously (Holmes and Harwood, 1937, 1932).

4.2. Whole-rock geochemistry

Major and trace element abundance data from two suites of Western Rift lava samples (Table 1) encompass 19 samples collected by the authors in 2013 and 41 samples from the classic Combe collection (Holmes and Harwood, 1937). We present new analyses and previously unpublished data for the Combe samples. Mafic Bufumbira lavas generally overlap with lavas erupted from the larger Virunga volcanoes in major element concentrations (Figs. 2 and 3), though the latter also extend to more evolved compositions, i.e., Gahinga, Karisimbi and Sabinyo lavas include K-trachytes and latites with <2% MgO and >60% SiO_2 (Rogers et al., 1998, 1992). Sabinyo lavas follow a slightly different trend than the rest of Virunga, characterized by lower alkali contents at high SiO_2 (Fig. 2). The mafic alkaline Bufumbira lavas comprise primarily potassic basanites with a few potassic hawaiites and mugearites (Fig. 2, Table 1). Toro Ankole lavas from both the Katwe-Kikorongo and Bunyaruguru fields are comparably alkaline but more silica-undersaturated, falling dominantly in the nephelinite field (Fig. 2). Lavas from both volcanic provinces are potassic (K_2O/Na_2O = 0.8–2.2 at Bufumbira, 0.3–2.7 at Toro Ankole), and most are nepheline and/or leucite normative despite the absence of these phases as large phenocrysts in the rocks.

Major element oxide variations displayed by the Virunga volcanoes are consistent with removal of olivine and clinopyroxene, and trend towards greater degrees of fractionation recorded by the most evolved samples from Karisimbi and Sabinyo (Fig. 3). Katwe-Kikorongo lavas are distinguished by higher CaO, TiO_2 and P_2O_5 and lower Al_2O_3 than any Virunga lavas. A cluster of Katwe-Kikorongo lavas have MgO ~10–12 wt%. This subset of lavas has a wide range in most major element oxides (Fig. 3) and therefore do not appear to be related by fractionation to a single common mafic parental composition.

Abundances of Ni, Cr, and Sc correlate positively with MgO overall, suggesting progressive removal of olivine and clinopyroxene; lavas with > ~ 12 wt% MgO and several of the Karisimbi PKBs (MgO = 7–13 wt%) have unusually high Sc contents (30–42 ppm) that suggest some clinopyroxene accumulation occurred in the most primitive lavas (Fig. 4). We observe no clear correlation for V, suggesting melting occurred in the presence of rutile or another Ti-bearing phase. Abundances of the incompatible trace elements Ba, La, and Zr correlate broadly negatively with MgO but, like the major element oxides, vary widely among the most primitive lavas (e.g., Ba ranges between 700 and 1600 among samples with 11–12 wt% MgO; Fig. 4); Ba, La, and Zr display strong positive correlations with one another across the entire compositional range of our samples.

Bufumbira, Katwe-Kikorongo and Bunyaruguru mafic lavas are all enriched in the most highly incompatible trace elements relative to OIB (Fig. 5). Each volcanic field has broadly consistent patterns of enrichment and depletion in individual elements, but the provinces are distinctly different from one another. Bufumbira mafic lavas have rather smooth patterns overall but display pronounced negative P anomalies as might be expected for melting in the presence of apatite. The elements Pb and Li show variable behavior across the province. Primitive samples (MgO >8 wt%) are depleted in Li (~5–9 ppm) while less magnesian bulk compositions are characterized by small positive Li anomalies (up to 22 ppm). Katwe-Kikorongo and Bunyaruguru samples have higher abundances of the most highly incompatible trace elements than the Bufumbira lavas. This latter suite is characterized by consistent negative K and P anomalies and strikingly uniform Ti contents, consistent with melting in the presence of phlogopite, amphibole, apatite and ilmenite. All of the lavas have steep (LREE enriched) REE profiles, particularly in Toro Ankole (La/Yb_n = 12–47 for Bufumbira, 59–132 for Katwe-Kikorongo and Bunyaruguru; Fig. 6); REE profiles are subparallel within each volcanic province but differ between the two provinces.

One lava analyzed for this study (BN-07-100) from the Bunyaruguru field of Toro Ankole is compositionally similar to Bufumbira lavas. This

Table 1
Major element oxide (wt%, normalized to 100% anhydrous) and trace element (ppm) concentrations for lavas. FeO* = total iron. K, Ti, and P calculated from major element analysis; all other trace elements determined by measurement with ICP-MS. Major elements determined by measurement with ICP-AES.

Sample	SiO_2	TiO_2	Al_2O_3	FeO*	MnO	MgO	CaO	Na_2O	K_2O	P_2O_5	Be	Sc	V	Cr	Co	Ni	Cu	Zn	Cs	Rb	Ba
Bufumbira																					
BU-01-100	45.58	3.24	13.72	11.1	0.18	9.25	10.16	2.45	3.58	0.60	1.92	8.5	181	466	46	168	56	99	1.17	128	1060
BU-02-100	45.67	3.26	13.26	11.3	0.19	9.47	10.47	2.22	3.39	0.60	1.88	29.1	296	427	51	184	65	285	0.97	90	1018
BU-04-100	44.96	2.62	11.52	11.0	0.19	13.91	9.42	2.58	3.04	0.55	2.05	16.1	158	888	61	402	110	98	1.15	131	1099
BU-04-101	44.02	2.78	10.68	11.4	0.20	14.48	10.09	2.50	3.11	0.59	2.00	26.9	250	832	66	327	60	93	0.95	82	815
BU-05-100	43.89	2.49	9.55	11.2	0.19	18.79	9.24	1.94	2.11	0.40	1.43	18.7	91	492	75	343	66	90	0.79	48	410
BU-06-100	48.66	2.60	13.54	9.7	0.17	9.74	9.72	2.24	2.96	0.52	1.60	29.3	248	698	43	101	22	105	0.96	117	919
BU-07-100	44.74	2.81	10.97	11.2	0.19	14.75	10.10	2.15	2.45	0.46	1.56	29.3	259	593	70	429	64	108	0.72	64	765
BU-08-100	49.73	2.91	13.91	9.7	0.17	7.40	9.16	2.67	3.60	0.54	2.41	11.6	155	272	35	66	32	93	1.93	146	1031
BU-09-100	53.73	2.16	17.97	7.8	0.16	2.57	5.65	3.69	5.33	0.81	3.00	6.2	86	0	13	1	10	94	0.46	86	1168
BU-10-100	48.95	3.20	16.69	10.6	0.18	4.99	7.53	2.80	4.21	0.65	2.17	20.3	241	68	33	16	16	118	1.59	385	1243
BU-11-100	49.00	3.16	16.09	10.3	0.16	5.85	8.59	2.50	3.69	0.52	1.97	10.2	168	164	35	34	25	93	1.26	121	1251
BU-13-100	44.46	3.79	14.34	11.7	0.21	7.08	10.22	2.98	4.20	0.78	2.37	21.2	214	148	40	53	37	108	1.54	173	1402
BUM-01	43.05	3.49	9.76	11.2	0.19	13.34	13.11	1.97	3.16	0.52	1.71	36.1	326	750	70	300	81	107	0.89	88	1028
BuR-01	46.42	3.06	12.71	11.1	0.19	10.69	9.49	2.36	3.14	0.62	1.57	22.6	221	406	47	166	40	102	0.79	76	786
C-1902	51.39	2.57	16.09	9.2	0.17	4.48	7.35	3.21	4.63	0.74	2.7	14.9	205	85	43	84	31	96	1.60	132	1238
C-1906	51.41	2.72	16.58	9.8	0.17	4.32	6.95	2.82	4.40	0.70	2.2	14.2	203	80	32	84	23	100	0.70	116	1257
C-2778	48.80	2.99	14.18	10.8	0.18	7.16	9.63	2.30	3.26	0.57	1.6	25.4	285	212	46	91	23	103	1.10	127	1175
C-2784	45.04	3.15	14.17	10.9	0.21	6.73	10.59	3.91	4.22	0.92	2.9	20.2	282	183	47	153	48	113	1.30	115	1470
C-2790	45.73	3.44	13.96	11.2	0.21	6.73	10.78	2.83	4.13	0.82	2.4	22	318	171	51	117	32	110	1.20	130	1344
C-2810	47.70	3.84	16.10	11.6	0.18	5.01	8.16	2.82	3.81	0.61	2	20.5	334	18	55	113	27	115	1.00	123	1361
C-2822	46.92	3.12	14.32	11.4	0.20	7.29	9.77	2.76	3.36	0.66	2.1	23.2	273	282	62	141	41	110	0.90	94	1081
C-2845	44.84	3.58	13.51	11.5	0.20	8.23	10.67	2.72	3.86	0.73	2.2	23.7	314	288	56	189	49	108	1.10	114	1277
C-2872	47.60	3.14	12.11	10.7	0.18	8.72	11.81	2.09	2.98	0.46	1.7	32.3	329	328	55	125	32	94	1.00	138	976
C-2907	48.48	2.51	15.98	8.4	0.20	2.68	8.83	5.30	6.71	0.73	4.1	8.6	242	12	38	69	40	100	2.10	176	1588
C-3042	50.79	2.82	15.49	9.5	0.17	5.26	8.00	3.03	4.08	0.67	2.6	15.8	215	146	57	101	34	97	1.80	162	1221
C-3044	54.29	2.07	17.97	7.7	0.16	2.66	5.63	3.83	5.13	0.41	1.7	4	66	3	13	23	8	44	0.80	72	1321
C-3045	44.79	3.59	13.66	11.6	0.20	7.99	10.70	2.73	3.74	0.77	2.2	23.5	311	271	70	183	53	110	1.10	105	1259
CV201	50.59	3.38	15.55	10.5	0.16	4.46	8.14	2.74	3.78	0.48	2.3	21.2	316	29	48	97	23	98	1.20	126	1245
CV767	41.84	5.51	11.87	12.3	0.20	6.76	11.41	2.89	6.27	0.76	2	19.8	347	137	82	228	170	117	1.80	190	1297
RG12847	45.99	3.57	16.56	11.8	0.20	4.87	9.25	3.51	3.42	0.63	2.2	14.3	280	28	51	124	61	111	1.10	94	1160
RG22779	46.82	3.43	17.72	10.7	0.19	3.25	9.33	3.71	3.87	0.76	2.4	11.9	196	7	46	98	63	104	1.30	105	1210
RG22783	46.10	3.61	16.65	11.5	0.19	4.26	9.60	3.53	3.75	0.66	2.2	15	287	6	46	112	62	111	1.10	96	1182

Sample	Th	U	Nb	Ta	K	La	Ce	Pb	Pr	Sr	P	Nd	Sm	Zr	Hf	Eu	Ti	Gd	Tb	Dy	Li	Y	Ho	Er	Tm	Yb	Lu
Bufumbira																											
BU-01-100	9.7	2.4	101	6.4	29,460	77	151	7.2	17	640	2598	64	10	253	6.8	2.79	19,222	9.3	1.2	5.78	6.7	25	1.06	2.87	0.39	2.46	0.36
BU-02-100	10.6	2.0	125	7.1	27,806	77	171	5.7	17	1022	2607	70	11	263	6.6	3.09	19,347	9.8	1.2	5.76	6.7	29	1.06	2.84	0.38	2.41	0.34
BU-04-100	29.6	3.2	118	7.2	24,709	99	189	7.8	21	728	2349	77	12	266	6.4	3.20	15,406	10.7	1.1	5.57	8.2	29	1.02	2.72	0.37	2.33	0.35
BU-04-101	11.6	2.5	123	6.8	25,419	79	168	2.3	16	973	2528	68	10	236	5.8	2.83	16,399	9.1	1.0	4.82	7.4	24	0.87	2.32	0.30	1.91	0.27
BU-05-100	14.5	1.4	38	2.3	17,481	31	60	5.1	7	246	1759	26	4	103	4.7	1.24	14,927	4.0	0.9	4.33	5.7	23	0.81	2.14	0.29	1.79	0.30
BU-06-100	11.0	1.7	91	4.8	24,551	68	152	7.1	14	786	2271	60	10	235	5.7	2.61	15,565	8.8	1.1	5.37	9.0	29	1.00	2.74	0.37	2.35	0.34
BU-07-100	7.8	1.4	88	4.8	20,327	54	121	5.5	12	745	2001	53	9	199	5.1	2.47	16,838	7.9	0.9	4.75	6.3	25	0.86	2.30	0.30	1.92	0.27
BU-08-100	15.9	3.3	95	6.0	29,735	83	161	10.2	18	628	2345	66	10	273	7.2	2.75	17,388	9.4	1.1	5.46	11.3	25	1.01	2.73	0.37	2.33	0.34
BU-09-100	34.8	4.3	142	8.7	43,931	109	215	15.5	25	1185	3532	87	13	394	9.2	3.35	12,854	11.5	1.3	6.34	14.1	31	1.17	3.22	0.44	2.79	0.40
BU-10-100	14.2	2.2	134	7.0	34,557	92	199	9.9	19	1017	2820	78	12	333	8.0	3.17	18,972	10.8	1.2	6.16	10.3	34	1.14	3.11	0.42	2.73	0.39
BU-11-100	16.5	2.5	92	5.8	30,292	77	152	8.4	17	890	2248	62	10	275	6.8	2.73	18,707	9.1	1.0	5.25	9.3	25	0.98	2.69	0.37	2.36	0.34
BU-13-100	25.6	2.9	143	9.2	34,473	111	217	8.4	24	1327	3356	89	14	338	7.8	3.84	22,499	12.6	1.4	6.61	8.1	35	1.21	3.21	0.43	2.75	0.40
BUM-01	7.4	1.5	101	4.7	26,153	63	142	4.7	14	911	2270	59	9	206	5.2	2.68	20,860	8.1	0.9	4.17	5.3	21	0.75	1.92	0.24	1.52	0.21
BuR-01	8.8	1.6	88	4.2	25,665	61	137	6.3	13	791	2656	55	9	211	5.1	2.31	18,060	7.5	0.9	4.22	6.6	23	0.78	2.08	0.27	1.75	0.25

(continued on next page)

Table 1 (*continued*)

Sample	Th	U	Nb	Ta	K	La	Ce	Pb	Pr	Sr	P	Nd	Sm	Zr	Hf	Eu	Ti	Gd	Tb	Dy	Li	Y	Ho	Er	Tm	Yb	Lu
C-1902	23.7	4.0	139	8.2	37,936	118	216	13.5	26	1190	3186	87	13	385	8.1	3.18	15,227	10.7	1.4	6.62	17.1	33	1.20	3.26		2.88	0.42
C-1906	20.6	2.9	135	8.0	35,943	110	206	13.6	25	1169	3011	84	12	380	8.2	3.12	16,066	10.2	1.4	6.51	11.8	33	1.21	3.34		2.79	0.44
C-2778	16.8	2.2	104	6.3	26,895	89	171	9.1	21	946	2487	71	11	311	7.1	2.85	17,805	9.2	1.3	6.26	9.3	30	1.13	3.01		2.59	0.38
C-2784	25.7	4.6	188	10.7	34,698	138	252	14.4	31	1557	3971	104	15	419	8.3	3.97	18,704	12.2	1.6	7.12	11.9	34	1.26	3.47		2.82	0.42
C-2790	19.3	3.5	155	9.4	34,615	116	217	9.9	26	1332	3622	90	14	355	7.7	3.42	20,802	11.0	1.4	6.66	12.3	31	1.19	3.10		2.54	0.39
C-2810	17.5	2.5	123	7.2	31,212	96	179	9.9	22	1002	2618	76	12	357	7.7	3.01	22,720	9.8	1.3	6.50	9.2	33	1.18	3.20		2.77	0.43
C-2822	15.2	2.7	120	7.3	27,891	93	177	8.1	22	1086	2880	75	11	333	7.2	2.92	18,704	9.3	1.3	6.30	8.4	31	1.17	3.10		2.63	0.41
C-2845	15.0	2.6	136	8.2	31,959	98	185	7.4	23	1208	3186	78	12	332	7.2	3.17	21,402	9.9	1.3	6.27	8.2	31	1.11	2.99		2.44	0.35
C-2872	12.3	2.2	92	5.6	24,571	73	142	6.2	18	800	2007	64	11	277	6.6	2.61	18,704	8.5	1.2	5.84	9.1	28	1.07	2.68		2.28	0.36
C-2907	33.6	4.7	221	10.1	55,119	162	277	15.6	32	2052	3142	100	14	431	7.9	3.44	14,867	11.6	1.4	6.24	18.1	30	1.12	3.13		2.59	0.40
C-3042	21.6	3.6	128	7.7	33,536	108	200	12.0	24	1196	2880	81	12	358	7.8	2.95	16,726	9.8	1.3	6.17	14.1	30	1.13	3.03		2.58	0.38
C-3044	13.6	2.5	79	4.7	41,588	68	124	8.0	15	1321	1746	48	7	224	4.8	1.75	12,110	6.0	0.8	3.57	9.1	18	0.66	1.76		1.58	0.24
C-3045	14.9	2.4	138	8.5	30,548	99	187	8.1	23	1213	3316	80	12	338	7.3	3.25	21,162	10.1	1.4	6.48	8.4	31	1.14	3.10		2.52	0.39
CV201	20.3	3.8	109	6.7	31,046	88	170	10.1	21	824	2095	72	11	325	7.6	2.79	20,083	9.2	1.3	6.54	14.4	31	1.18	3.16		2.68	0.40
CV767	20.7	4.0	193	13.0	51,549	129	242	2.8	30	1387	3273	100	14	287	7.2	3.43	32,732	11.1	1.3	5.69	7.5	25	0.98	2.57		1.93	0.28
RG12847	13.3	2.5	117	7.2	28,306	83	159	6.9	20	1076	2749	68	11	325	6.7	2.96	21,342	9.1	1.3	6.29	9.6	31	1.14	3.10		2.60	0.37
RG22779	14.2	2.7	127	7.7	31,046	89	168	7.7	21	1147	3186	72	12	348	7.0	3.14	19,903	9.4	1.3	6.57	9.9	32	1.20	3.22		2.74	0.41
RG22783	14.0	2.7	120	7.5	30,714	86	164	7.3	20	1094	2836	71	11	335	7.1	3.02	21,402	9.4	1.3	6.48	10.0	32	1.21	3.19		2.71	0.39

Sample	SiO_2	TiO_2	Al_2O_3	FeO*	MnO	MgO	CaO	Na_2O	K_2O	P_2O_5	Be	Sc	V	Cr	Co	Ni	Cu	Zn	Cs	Rb	Ba
Katwe-Kikorongo																					
KK-24-100	39.6	6.22	10.49	14.6	0.3	5.86	15.1	4.00	2.21	1.36	4.07	13.6	324	6	44	26	169	140	1.69	60	1209
KK-25-102	41.6	5.66	11.15	13.3	0.24	6.43	13.1	2.68	4.55	1.09	3.26	13.1	396	211	41	87	122	119	1.34	191	2450
KK-28-101	41.7	5.39	5.8	14.4	0.19	11.63	17.54	1.15	1.55	0.41	1.54	28.0	208	373	55	102	88	89	0.43	57	788
KK-31-100	46.6	4.17	8.7	11.8	0.18	10.43	13.2	2.97	1.26	0.52	2.15	33.1	200	506	49	123	122	90	2.20	53	1212
C-5631	41.5	4.98	6.51	13.6	0.2	11.40	17.2	1.58	2.31	0.43	1.6	40.7	309	364	62	163	99	100	0.60	64	945
C-5635	41.7	5.13	6.73	13.6	0.2	10.89	16.9	1.71	2.49	0.43	1.6	42.3	338	399	71	177	119	109	0.60	71	938
C-5763	41.0	5.60	9.46	13.3	0.3	5.76	16.5	2.62	4.00	1.34	3.2	19.2	367	36	47	134	165	134	1.00	102	1741
C-5764	42.6	5.30	11.17	12.5	0.25	5.25	13.4	2.98	5.18	1.22	3.8	14.1	343	54	43	63	101	131	1.30	131	1737
C-5783	42.6	5.23	11.0	12.5	0.3	5.53	13.21	3.11	5.07	1.26	3.8	15.3	308	65	57	69	107	135	1.30	114	1692
C-5809	39.1	5.46	7.8	12.8	0.2	10.85	16.40	2.02	4.03	1.10	2.5	27.7	350	367	65	168	166	116	0.70	96	1463
C-5811	38.8	5.46	7.9	13.0	0.2	10.83	17.50	1.60	3.58	0.96	2.4	27	334	332	72	152	155	110	0.70	97	1655
C-5812	38.9	5.51	8.0	12.7	0.2	9.97	16.76	2.26	4.47	0.94	2.7	27.8	333	286	61	143	166	117	0.90	102	1450
C-5813	39.4	5.32	8.6	12.6	0.2	8.36	16.55	2.71	4.88	1.14	3.1	23.6	311	174	55	110	169	120	0.60	96	1666
C-5826	44.9	4.77	9.8	12.3	0.2	8.59	12.24	5.00	1.30	0.63	2.5	21	334	302	67	180	144	122	2.00	70	1444
C-5829	41.4	4.99	7.2	12.5	0.2	12.16	14.70	2.84	3.13	0.67	3.1	25.3	288	393	59	218	146	115	0.30	73	1687
C-5830	51.4	2.81	12.4	10.2	0.2	6.09	10.78	1.47	3.81	0.63	3.6	23.3	189	145	37	129	71	78	1.20	96	1178
C-5839	39.9	5.74	8.1	14.1	0.2	8.67	18.31	1.52	1.90	1.22	3	25.3	309	149	55	116	166	126	0.20	50	1949
C-5854	41.3	5.33	6.7	12.9	0.2	11.86	17.66	1.53	1.93	0.42	1.9	35.2	313	368	64	172	147	112	0.50	53	1094
C-5862	40.7	5.10	7.3	12.9	0.2	12.14	14.65	1.62	4.31	0.84	2.3	25	310	565	76	282	145	121	0.40	86	1389
C-5880	39.4	5.68	7.7	13.4	0.2	11.10	16.34	1.97	3.30	0.68	2.4	26.5	348	369	66	231	162	129	0.30	76	1427
C-5881	39.3	5.60	7.7	13.0	0.2	11.17	15.71	1.88	4.32	0.87	2.6	27.3	345	379	63	176	169	125	0.50	88	1451
C-5901	41.0	5.28	7.7	12.9	0.2	12.59	14.59	1.24	3.75	0.51	2.3	25.8	335	510	73	241	161	122	0.70	91	1593
C-5924	44.6	4.56	8.6	12.1	0.2	9.86	14.18	3.45	1.71	0.64	2.1	28.1	324	347	59	148	106	107	5.50	109	1892
Bunyaruguru																					
BN-07-100	42.22	5.24	8.04	10.3	0.14	16.57	9.13	1.10	6.83	0.27	1.45	22.7	164	864	69	503	96	97	0.66	174	1615

Sample	Th	U	Nb	Ta	K	La	Ce	Pb	Pr	Sr	P	Nd	Sm	Zr	Hf	Eu	Ti	Gd	Tb	Dy	Li	Y	Ho	Er	Tm	Yb	Lu
Katwe-Kikorongo																											
KK-24-100	52.2	11.6	300	17.8	17,375	232	445	11.8	49	4014	5627	171	23.0	538	12.7	5.96	35,336	18.8	1.7	6.64	10.4	30	1.04	2.62	0.30	1.79	0.24
KK-25-102	35.5	4.5	315	18.9	36,152	290	563	10.1	61	3478	4553	215	29.4	620	9.7	7.66	32,491	23.8	1.3	5.34	8.5	24	0.86	2.18	0.26	1.57	0.22
KK-28-101	19.5	2.4	103	7.2	12,540	84	175	4.1	20	1555	1734	75	10.7	215	6.4	2.83	31,410	8.5	0.8	3.10	4.3	13	0.47	1.16	0.13	0.78	0.11
KK-31-100	38.2	2.4	133	8.6	9933	114	225	7.9	25	3571	2166	90	12.2	249	7.1	3.13	23,669	10.0	1.0	3.94	7.6	18	0.64	1.64	0.20	1.21	0.17
C-5631	11.5	2.0	120	7.9	19,009	88	176	4.1	22	1275	1876	78	10.7	256	6.2	2.67	29,674	7.9	0.9	3.08	4.6	12	0.47	1.24		0.77	0.12
C-5635	13.3	2.3	129	8.9	20,503	98	199	4.3	25	1241	1876	88	12.0	234	6.1	2.91	30,514	8.8	0.9	3.36	4.7	13	0.51	1.35		0.82	0.11
C-5763	36.1	9.2	319	18.8	32,789	256	478	11.3	59	3306	5760	191	24.9	455	10.7	6.23	33,092	20.2	2.0	6.88	8.9	24	1.01	2.68		1.65	0.23
C-5764	30.2	6.1	283	16.2	42,916	207	383	13.3	47	3078	5324	156	20.6	503	11.3	4.98	31,713	15.8	1.7	6.43	14.7	25	1.04	2.78		1.85	0.27
C-5783	28.4	4.4	279	15.7	41,837	201	367	13.6	45	2635	5455	150	19.8	511	11.0	4.84	31,173	15.3	1.7	6.20	9.9	25	0.99	2.70		1.83	0.27
C-5809	24.1	5.6	239	13.1	32,955	181	347	10.2	43	2335	4713	147	19.6	404	8.7	4.72	32,252	14.5	1.5	5.20	7.3	19	0.76	2.01		1.09	0.15
C-5811	23.6	6.6	232	13.1	28,721	176	337	7.6	42	2205	4058	144	19.4	378	8.5	4.70	31,593	14.2	1.5	5.21	7.2	18	0.76	1.93		1.08	0.16
C-5812	25.5	5.9	246	13.8	36,524	187	358	6.5	45	2337	4058	152	20.9	415	8.9	4.96	32,552	15.3	1.6	5.42	7.9	19	0.80	2.09		1.22	0.16
C-5813	25.8	6.8	266	14.2	40,675	197	363	10.5	45	2716	4975	151	20.4	482	10.2	5.01	32,012	15.6	1.6	5.79	9.2	21	0.86	2.29		1.38	0.18
C-5826	26.4	5.4	214	13.0	10,542	168	322	7.3	40	1945	2706	128	16.6	343	8.1	4.22	27,936	13.7	1.3	4.71	8.8	18	0.72	1.94		1.28	0.19
C-5829	19.3	4.0	209	12.8	25,733	145	281	9.0	35	2441	2880	121	16.0	435	9.5	3.96	29,615	12.1	1.3	4.63	9.1	17	0.71	1.88		1.19	0.17
C-5830	19.8	4.0	141	8.0	31,212	108	214	9.1	27	1065	2706	91	13.2	267	6.5	3.34	16,666	10.8	1.1	4.59	11.9	18	0.73	1.88		1.31	0.18
C-5839	19.7	4.9	249	14.3	15,357	167	309	1.4	38	3908	5193	127	17.2	399	9.4	4.27	33,571	13.2	1.4	4.98	9.1	19	0.77	2.00		1.27	0.17
C-5854	18.0	10.7	165	10.5	16,187	125	244	4.9	31	1682	1833	105	14.0	310	7.8	3.46	32,312	10.5	1.1	3.90	6.0	14	0.59	1.48		0.91	0.13
C-5862	15.8	4.0	202	12.0	35,279	140	268	5.9	33	1753	3622	110	14.7	354	8.5	3.86	30,154	11.8	1.2	4.36	6.5	16	0.64	1.69		1.07	0.15
C-5880	19.9	5.4	237	14.0	26,646	163	318	1.6	40	2235	2880	133	18.0	385	9.2	4.60	33,151	14.3	1.4	5.20	8.1	19	0.77	2.04		1.29	0.19
C-5881	20.7	4.4	235	14.2	36,026	165	318	1.8	40	2385	3796	136	18.2	388	9.1	4.36	33,691	13.4	1.4	5.14	7.8	20	0.78	2.15		1.36	0.19
C-5901	15.9	3.0	201	12.6	30,548	132	261	5.4	32	2283	2182	111	15.0	318	8.3	3.74	31,113	11.2	1.2	4.37	7.2	17	0.68	1.79		1.10	0.17
C-5924	21.0	2.8	149	10.9	14,029	141	269	6.4	33	1822	2749	109	14.4	292	7.0	3.58	27,037	11.1	1.1	4.09	7.3	16	0.64	1.70		1.09	0.17
Bunyaruguru																											
BN-07-100	12.0	2.4	177	10.5	55,085	106	232	4.7	22	1271	1138	90	12.0	239	6.9	3.30	30,518	9.5	0.8	3.07	5.5	12	0.47	1.16	0.12	0.78	0.11

sample lacks the K depletion and extreme REE enrichment of the Katwe-Kikorongo lavas, producing a primitive-mantle normalized profile similar to those of the Bufumbira samples (Fig. 5).

4.3. $^{40}Ar/^{39}Ar$ age dating

The measured $^{40}Ar/^{39}Ar$ eruption ages for the Bufumbira lavas are primarily <130 ka but range from 20 to 662 ka. The two Toro Ankole samples have ages of 87 ka (Katwe-Kikorongo) and 188 ka (Bunyaruguru) (Table 2). Errors are relatively large for some samples ($2\sigma = 1.0$ ka–74.6 ka for plateau ages), possibly due to ^{39}Ar recoil in groundmass (e.g. Koppers et al., 2000). Argon step heating plateau figures and detailed data table are in the supplementary information. Plateau ages from incremental step heating provided the lowest uncertainties and are preferred for the whole-rock (groundmass) samples; normal and inverse isochron ages were generally within uncertainty of the plateau ages with greater errors. Single crystal total fusion analyses for phlogopite separates from BU-09-100 yield an ideogram (probability density plot) age of 67.4 ± 12.4 ka and a total fusion age of 297.1 ± 109.3 ka; the incremental step heating age for this biotite (57.8 ± 5.0 ka) is preferred.

5. Discussion

Despite their proximity, primitive cinder cone fields from the Toro Ankole and Virunga Provinces display notable geochemical and, by extension, petrogenetic differences. These contrasting compositional features illuminate the spectrum of mantle enrichment and melting occurring beneath the Western Rift and inform our understanding of lithospheric structure in the region.

5.1. Post-melting processes

5.1.1. Crustal contamination

Primitive (>8% MgO) Bufumbira and Katwe-Kikorongo lavas do not display significant evidence for crustal contamination. At Katwe-Kikorongo, the country rock consists of a Paleoproterozoic mobile belt, dominated by basement gneiss and other high grade metamorphic rocks, while in Bufumbira the volcanics erupted through the Kibaran belt containing lower-grade metasediments of the Karagwe-Ankolean belt (Link et al., 2010). No evidence for significant assimilation of either of these materials is observed in our data. The lavas lack anomalous Pb enrichment (Ce/Pb > 20) and most have Nb/U > 35 and Sr/Ce < 12, within the range of expected values for mantle-derived melts (Hofmann et al., 1986; Sun and McDonough, 1989). While the generation of evolved lavas elsewhere in the Virunga province (e.g., Sabinyo) has been attributed to contamination (De Mulder and Pasteels, 1986; Rogers et al., 1998), the large volcanic edifices erupting those lavas are structurally quite different from the cinder cone fields discussed here. The distinctive morphology and eruptive style at Bufumbira support magma transport through immature magmatic plumbing systems associated with monogenetic cinder cones and allow for only limited crustal interaction. Rapid magma transport to the surface is favored by immature magmatic pathways and could additionally explain the lack of crustal assimilation; Chakrabarti et al. (2009b) found that U-Th-Ra-series isotopes from young lavas of Nyiragongo volcano in Virunga were indicative of timescales of 4–6 ka from partial melting to eruption, evidence that rapid ascent is occurring within the volcanic province.

5.1.2. Fractionation

Bufumbira lavas with less than ~8 wt% MgO define major element trends consistent with fractionation of olivine and clinopyroxene from parental melts (Fig. 3). Samples with 8–18 wt% MgO appear to be individual primitive melts with variable but minor amounts of olivine and clinopyroxene accumulation (particularly BU-05-100, BU-07-100). In contrast, the Katwe-Kikorongo lavas lack clear linear trends among

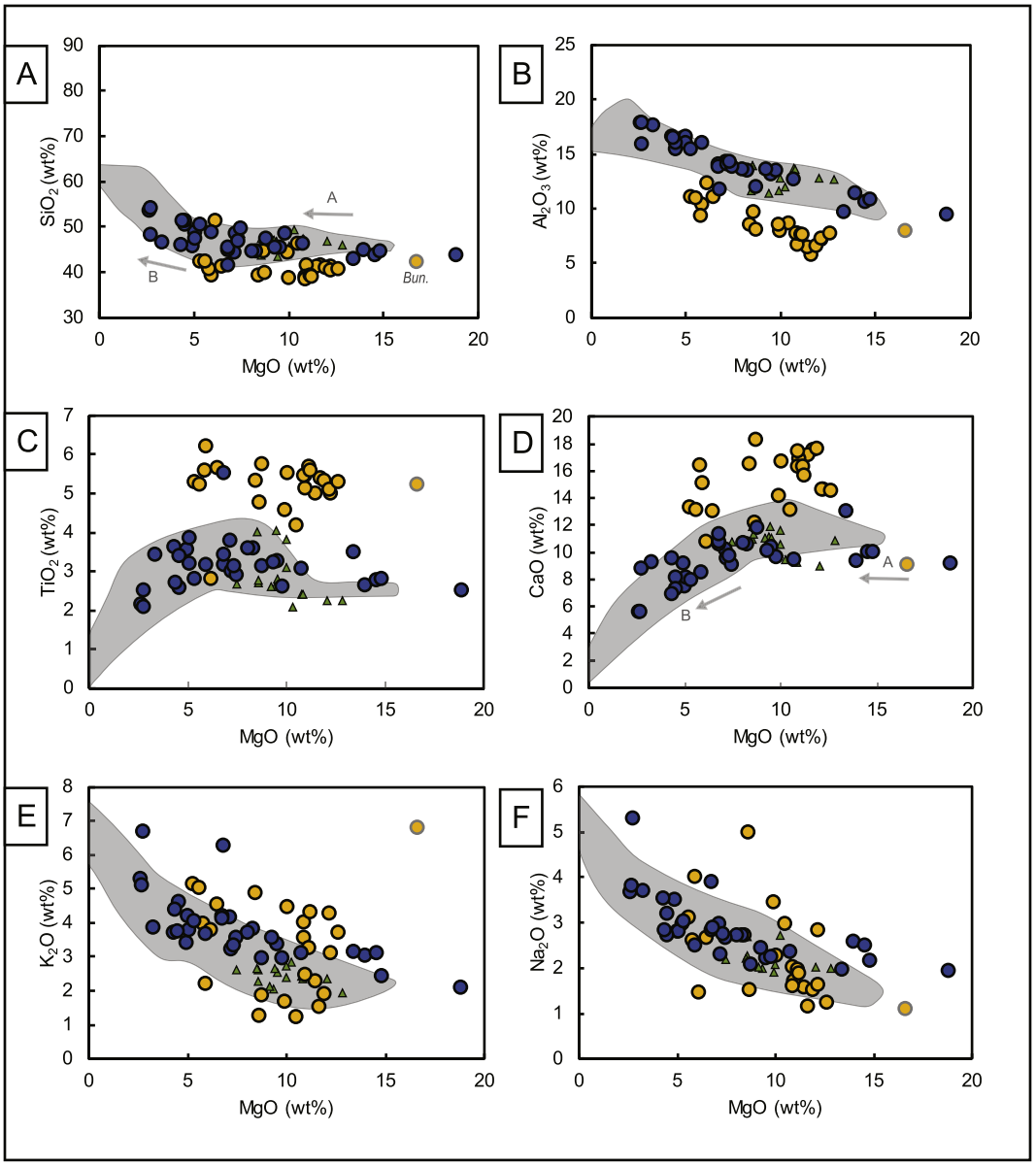

Fig. 3. Major element variation diagrams for Katwe-Kikorongo, Bunyaruguru, Bufumbira, and Karisimbi PKB lavas. Lavas from the other Virunga volcanoes are represented by gray fields. Symbols and data sources same as Fig. 2. Approximate fractionation trends are shown for primitive lavas >8% MgO (trend A; high-Mg olivine and clinopyroxene) and more evolved compositions <8% MgO (trend B; lower-Mg olivine and clinopyroxene, high-An plagioclase, ilmenite, spinel, rutile and magnetite) on selected plots (see Section 5.1 for discussion).

major elements (Fig. 3) and do not appear to define a coherent fractionation sequence.

We tested the plausibility of fractionation at Bufumbira with a linear least squares mixing model (Bryan et al., 1969; Carr and Gazel, 2017) using phenocryst mineral compositions determined through electron microprobe analysis using a Cameca SX-5 at Penn State University (Table 3). Results indicate that while some pairs of Bufumbira whole-rock sample compositions may be related through fractional crystallization, the samples do not define a suite of lavas derived from a single parental melt. In general, less evolved samples (e.g. basanites) appear to be related to inferred parental melts through <30% fractionation of high-Mg olivine ($Fo_{80–90}$) and clinopyroxene (Mg# = 80–90). More evolved samples (e.g. alkali basalts, K-hawaiites, K-mugearites) can be related to one another by (~30–40%) fractionation of lower-Mg# olivine (<Fo_{80}) and pyroxene (Mg# = 73–83), along with occasional small amounts of high-An plagioclase (~An_{90}), ilmenite, spinel, rutile and magnetite. Adding small amounts of nepheline to the fractionating assemblage improves fits for many calculations throughout the compositional spectrum.

We identify two distinct fractionating series (from parental magmas resembling high MgO samples BU-04-101 and BU-06-100) from which the evolved Bufumbira lavas can plausibly be related through fractionation, though the heterogeneous bulk lava compositions make it likely that more than two parental melt compositions are represented. The calculations suggest that samples BU-05-100 and BU-07-100 have accumulated olivine, i.e., they have anomalously high MgO and mixing calculations produce negative values for olivine fractionation; olivine in these lavas is also high-Fo and consistent with formation at high pressures. Assuming a model of Rayleigh fractionation and a bulk distribution coefficient determined from the normative mineralogy of the high-Mg lavas (without accumulated olivine), enrichment in highly incompatible elements (e.g. Zr, Ba, Rb, Sm) in daughter lavas are consistent with the fractionation sequences determined from least-squares mixing and support 10–40%

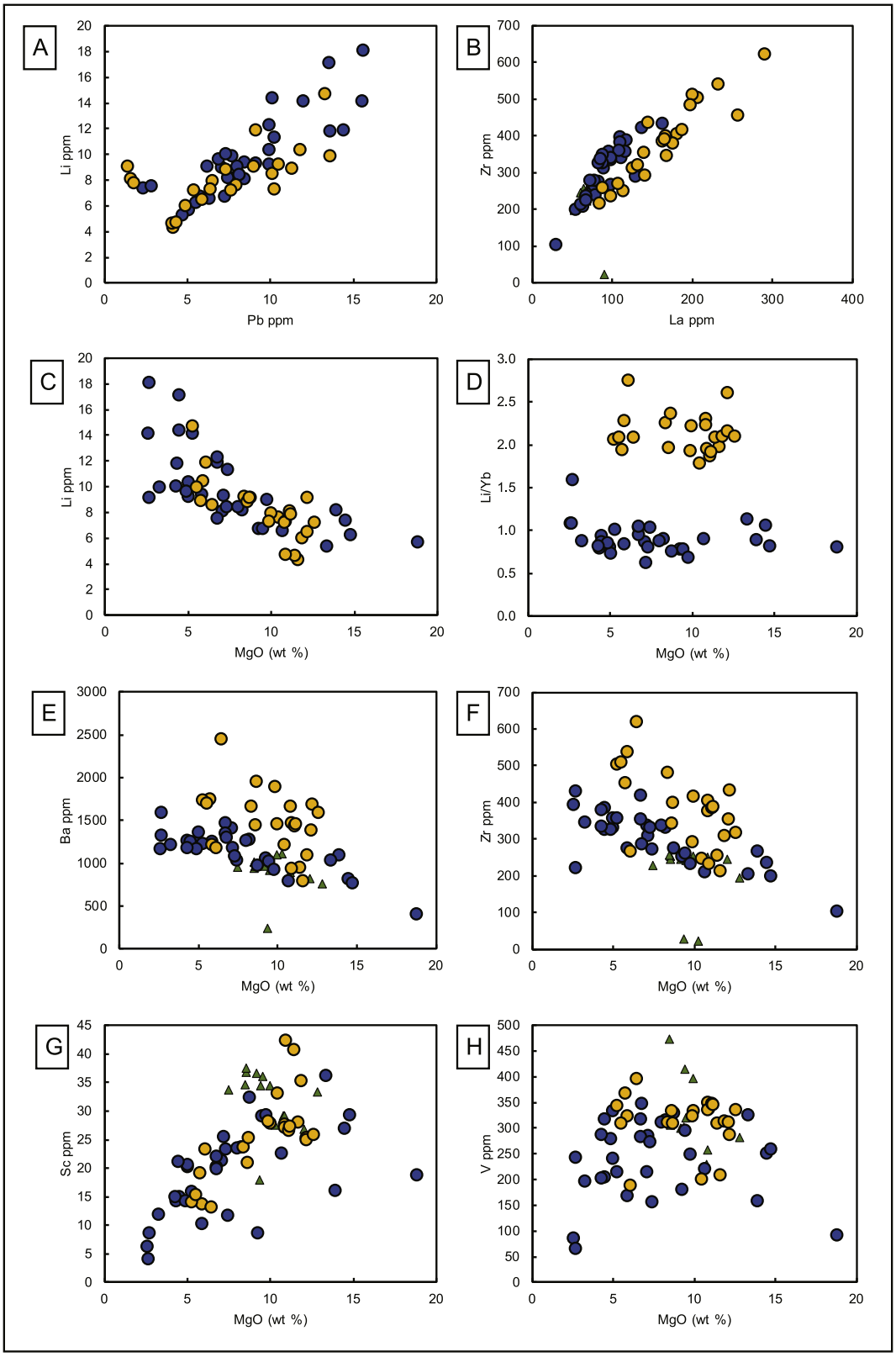

Fig. 4. Incompatible and compatible trace element variations relative to MgO in Bufumbira, Toro Ankole, and PKB lavas. These data are consistent with removal of olivine and clinopyroxene from parental melts, and with some olivine and clinopyroxene accumulation in the most MgO-rich melts.

fractionation from the more magnesian to more evolved compositions. BUM-01 and BUR-01, located farthest from the rift axis and outside the Bufumbira field proper, could not be successfully related to each other or to other primitive Bufumbira lavas through fractional crystallization through least-squares mixing calculations and are therefore interpreted as individual melt events.

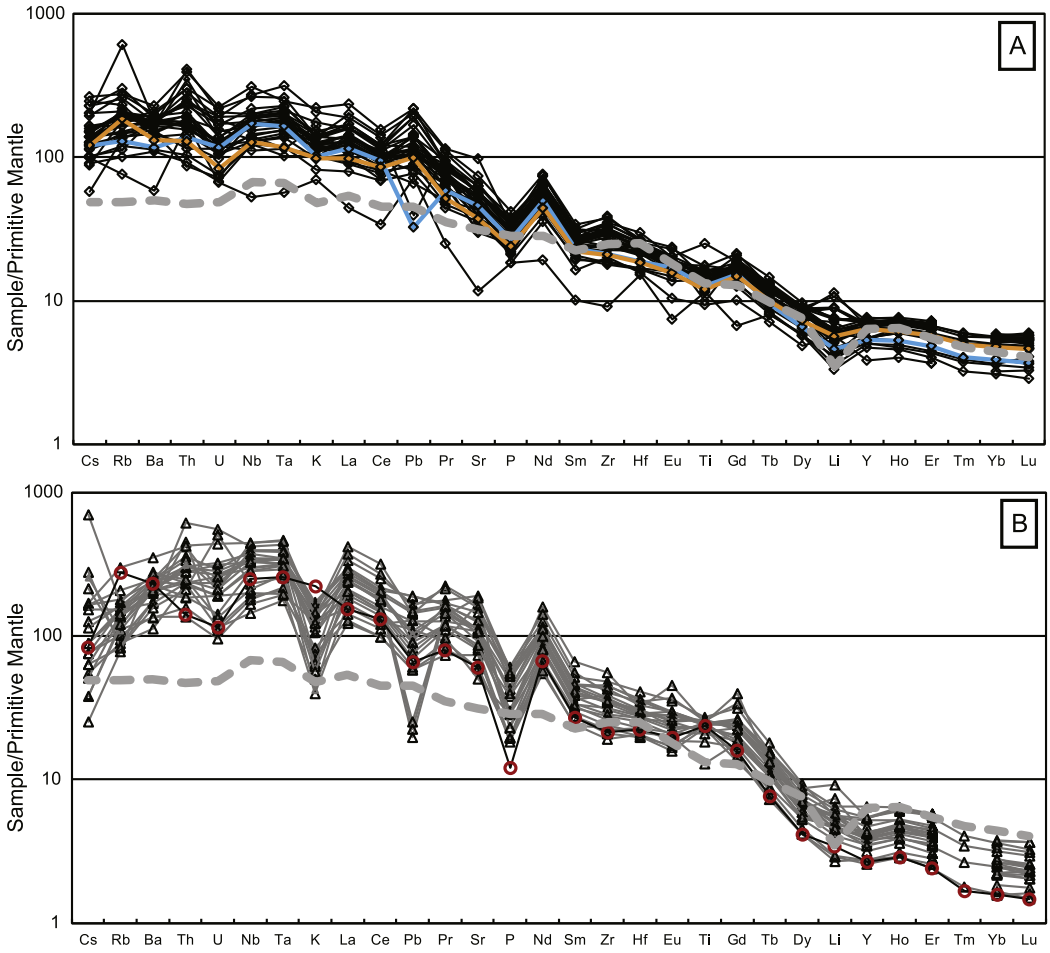

Fig. 5. Primitive mantle-normalized trace element concentrations for A) Bufumbira lavas with potential parental lavas BU-04-101 (blue) and BU-06-100 (orange) highlighted. and B) Toro Ankole lavas (Bunyaruguru and Katwe-Kikorongo volcanic fields). Bunyaruguru lava BN-07-100 highlighted with red circles. Gray dashed line represents OIB compositions on both plots. Both regions display enrichment in the most highly incompatible trace elements; Katwe-Kikorongo samples are characterized by higher degrees of enrichment, marked K, P and occasionally Pb depletions, and greater depletion of MREE and HREE relative to LREE. Concentrations normalized to primitive mantle of Sun and McDonough (1989). (For interpretation of the references to colour in this figure legend, the reader is referred to the web version of this article.)

5.2. Eruption geochronology and compositional evolution

In Bufumbira we identify three phases of volcanism among the samples dated for this study, suggesting that the cinder cone field did not form from a single pulse of magmatism. The oldest phase of volcanism has ages 663–110 ka, as measured in samples BU-05-100, BU-07-100, and BU-04-101. The off-rift Bufumbira lavas, BUM-01 and BUR-01, which erupted 10–20 km east of the main volcanic field, were dated to 56–60 ka, though the BUM-01 age has a very large uncertainty. The youngest phase of volcanism is recorded in samples BU-01-100, BU-06-100, BU-09-100, and BU-11-100 with ages between 20 and 23 ka. The ages measured for the primitive lavas from Bufumbira span the range of ages previously reported for most of the major volcanic edifices in Virunga (10–176 ka; De Mulder and Pasteels, 1986; Rogers et al., 1998); Mikeno has reported dates of up to 2.6 Ma (Kampunzu et al., 1998). In Bufumbira, the oldest lavas (~110–660 ka) lie in the central portion of the volcanic field (Fig. 10). The youngest lavas (~20–22 ka) are found throughout the main portion of the Bufumbira field and overlap geographically with the earliest phase of volcanism.

Whole rock major element trends among these Bufumbira samples record consistent geochemical variations over time. MgO and Ni contents decrease from older to younger lavas, while Al_2O_3 and total alkalis increase, consistent with greater degrees of magmatic evolution through fractionation throughout the history of the volcanic field (Fig. 11). The oldest lavas (BU-04-101, BU-05-100, and BU-07-100) include samples which have the highest MgO and appear to have accumulated high Fo olivine antecrysts that grew at greater depth and higher temperatures than equilibrium phenocrysts (Pitcavage et al., in preparation). Potential trace element indicators of depth and degree of melting (Tb/Yb and La/Yb), degree of carbonatitic metasomatism (Ti/Eu and Zr/Hf) or crustal contamination (Ce/Pb) do not vary systemically with age, suggesting that source composition and melting conditions do not vary significantly; rather, the data are consistent with a transition over time from accumulation of high-P and -T antecrysts—in equilibrium with more primitive melt compositions—to more evolved phenocrysts as more mature magmatic pathways allowed for increased crystallization.

The Toro Ankole lavas dated for this study are older than any previously reported ages for the province (predominantly K-Ar ages) except for one sample from Bagdasaryan et al. (1973; reported in Kampunzu et al., 1998) of 0.45 Ma. These ages demonstrate that while primitive volcanism in Toro Ankole appears to have been concentrated in the last ~50 ka, older eruptions were occurring, particularly in the Bunyaruguru region.

The sample from Toro Ankole's Bunyaruguru volcanic field (BN-07-100) is geochemically distinct from the rest of that volcanic province, with less extreme LREE/HREE enrichment (Fig. 4). It is also older than the dated Katwe-Kikorongo lava (189 ka vs. 87 ka). The Bunyaruguru

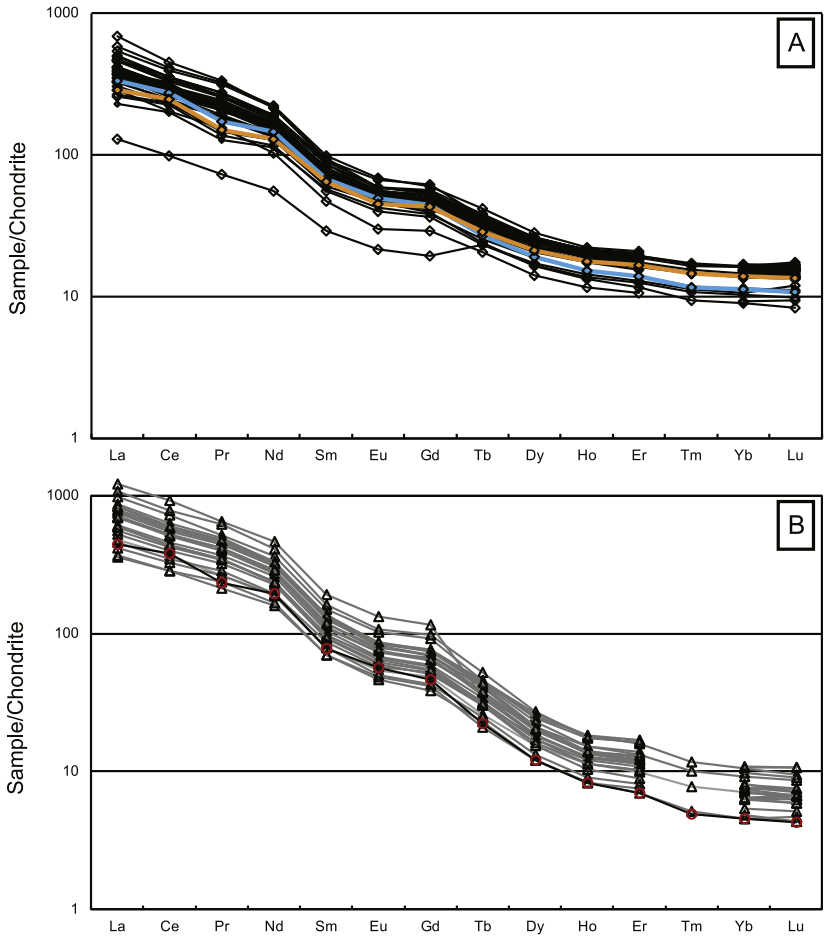

Fig. 6. Chondrite-normalized rare earth element concentrations for A) Bufumbira and B) Toro Ankole (Bunyaruguru and Katwe-Kikorongo volcanic fields) lavas. Symbols as in Fig. 4. Normalized to chondrite values of Sun and McDonough (1989).

field is located on the plateau east of the main rift valley in the southeastern portion of Toro Ankole, while Katwe-Kikorongo is more centrally located in the province, within the rift closer to the rift axis. Crustal thickness as determined by receiver function analysis is greater in the eastern portion of Toro Ankole (Wölbern et al., 2010), as well as to the north where lithospheric links to the Congo Craton have been inferred (Link et al., 2010). This raises the intriguing question of whether or not the early volcanism in the province was focused away from the eventual locus of rifting; unfortunately, these data do not provide enough resolution to fully address this issue.

5.3. Lithospheric melting in the Western Rift

5.3.1. Source mineralogy

Fundamental constraints on the mineralogy of the local lithospheric mantle come from abundant xenoliths found in this region (Lloyd, 1987, 1981), including some hosted in the lavas studied here (Nelson et al., 2015). Katwe-Kikorongo xenoliths present a diverse suite of lithologies. They are dominantly pyroxenitic with a few glimmerites (phlogopite-dominated), and contain varying amounts of titanite, perovskite, amphibole, and phlogopite—similar to MARID-type xenoliths (Dawson and Smith, 1977). Bufumbira xenoliths are also dominantly pyroxenites with a few peridotites; phlogopite is present in some samples. Garnet has not been observed in xenoliths from either province. The relationship between these xenoliths and their host lavas is complex (e.g. Muravyeva et al., 2014), and they are unlikely to be cognate, but their presence confirms hydrous alkali pyroxenite at depths within or above the range of melt generation beneath these regions; in Toro Ankole, it is particularly likely that the lavas originated beneath the depths at which these xenoliths are derived.

The primitive lavas described here provide additional important information on the magma source mineralogy. To first order, the source of lavas from both provinces is inferred to be lithospheric mantle consisting of pyroxene-rich mantle lithologies. Primitive lavas from both Virunga and Toro Ankole have Zn/Fe ($x10^4$) values of 10–15 (Fig. 7), elevated above expected values for melting of peridotite (8–10) and require the involvement of a pyroxenitic source (Le Roux et al., 2011, 2010). The Karisimbi PKBs overlap with Bufumbira in Zn/Fe, but also extend to lower values (7–13) within the range expected for peridotite melting, perhaps indicating greater contributions from peridotite in southern Virunga.

Lavas from both Virunga and Toro Ankole have $(Tb/Yb)_n$ ratios exceeding 1.8, typically suggestive of residual garnet following melting (Wang et al., 2002): garnet will preferentially retain HREE, leading to elevated MREE/HREE ratios (Fig. 8). In Bufumbira lavas, this ratio is slightly elevated (2.0–3.2). Clinopyroxene can also retain HREE during low-degree melting of near-solidus spinel lherzolite (Blundy et al., 1998). Given our observations of pyroxenitic xenoliths, the REE patterns in mafic Bufumbira lavas are best explained by melting of a clinopyroxene-rich spinel-facies lithospheric mantle, possibly close to the spinel-garnet transition with minor garnet influence. At Toro Ankole, $(Tb/Yb)_n$ is notably higher (3.6–6.4), a stronger indication of melting at depths of garnet stability. While garnet has not been observed in Toro Ankole xenoliths, perovskite and titanite are present, both of which may also play a contributing role in controlling REE systematics (e.g. Lloyd et al., 1996; Pilet et al., 2011). The Th/U ratio is

Table 2
$^{40}Ar/^{39}Ar$ dating results for Bufumbira, Katwe-Kikorongo, and Bunyaruguru samples. Notes: Sample irradiation 18-OSU-01 with FCT-NM (Kuiper et al., 2008). Age equations of Min et al. (2000). ±2σ (i): Analytical error; ±2σ (f): Full external error. N: Total heating steps; n: Heating steps included in age calculation; MSWD: mean square of weighted deviations; P: probability of fit. Preferred ages shown in bold.

					Plateau										Normal Isochron						
Sample Name	Material	Experiment Type	Age Type	Notes	Age (ka)	±2σ (i)	±2σ (f)	^{39}Ar	K/Ca	±2σ	MSWD	P	n	N	Age (ka)	±2σ (i)	±2σ (f)	$^{40}Ar/^{36}Ar$ intercept	±2σ	MSWD	P
BU-01-100	Groundmass	Incremental Heating	Plateau		**22.9**	**±13.2 ka**	±13.2 ka	91%	0.033	±0.022	0.90	56%	15	20							
BU-04-101	Groundmass	Incremental Heating	Plateau	Subatmospheric Initial $^{40}Ar/^{36}Ar$ = 294.00 ± 2.35 (SD).	**112.3**	**±72.8 ka**	±72.9 ka	66%	0.011	±0.005	0.89	55%	12	21	20.5	±158.3 ka	±158.3 ka	297.11	± 4.58	1.35	19%
BU-05-100	Groundmass	Incremental Heating	Mini Plateau		**662.5**	**±53.3 ka**	±55.3 ka	37%	0.190	±0.006	0.21	96%	6	25	650.4	±79.0 ka	±80.4 ka	296.08	± 2.86	0.22	93%
BU-06-100	Groundmass	Incremental Heating	Plateau	Excess Initial $^{40}Ar/^{36}Ar$ = 300.46 ± 0.76 (SD).	**22.4**	**±1.2 ka**	±1.3 ka	100%	0.334	±0.109	0.94	55%	25	25	22.4	±1.7 ka	±1.8 ka	300.39	± 1.52	1.07	37%
BU-07-100	Groundmass	Incremental Heating	Plateau	Subatmospheric Initial $^{40}Ar/^{36}Ar$ = 288.92 ± 3.14 (SD).	**125.6**	**±19.1 ka**	±19.3 ka	81%	0.172	±0.041	1.73	5%	14	26	126.9	±34.9 ka	±35.0 ka	287.98	± 7.15	2.52	0%
BU-09-100	Groundmass	Incremental Heating	Plateau		**21.5**	**±1.0 ka**	±1.1 ka	100%	0.600	±0.206	0.83	71%	27	27	20.7	±1.6 ka	±1.7 ka	297.90	± 4.02	0.81	74%
BU-09-100	Biotite	Total Fusion	Ideogram		39.4	±18.2 ka	±18.3 ka	86%	8.628	±0.827	2.39	0%	20	24	25.6	±37.6 ka	±37.6 ka	296.79	± 3.77	2.40	0%
BU-09-100	Biotite	Total Fusion	Total Fusion		431.9	±679.8 ka	±679.8 ka	59%	−3.347	±2.421	36.80	0%	9	18							
BU-09-100	Biotite	Incremental Heating	Plateau		**57.8**	**±5.0 ka**	±5.2 ka	100%	29.174	±5.459	0.83	75%	34	36	57.6	±17.1 ka	±17.1 ka	295.49	± 2.30	0.84	72%
BU-11-100	Groundmass	Incremental Heating	Plateau	Excess Initial $^{40}Ar/^{36}Ar$ = 298.37 ± 2.04 (SD).	**20.9**	**±2.3 ka**	±2.4 ka	100%	1.439	±0.191	0.15	100%	27	27	20.9	±4.1 ka	±4.1 ka	298.35	± 4.08	0.17	100%
BU-11-100	Plagioclase	Incremental Heating	Plateau	Excess Initial $^{40}Ar/^{36}Ar$ = 402.18 ± 32.62 (SD).	13.8	±11.1 ka	±11.1 ka	100%	0.093	±0.000	1.06	39%	17	17	1.4	±26.6 ka	±26.6 ka	407.33	±55.79	1.43	12%
BUM-01	Groundmass	Incremental Heating	Plateau		56.0	±74.6 ka	±74.6 ka	76%	0.015	±0.008	0.29	94%	7	18							
BUR-01	Groundmass	Incremental Heating	Mini Plateau		**59.8**	**±6.2 ka**	±6.4 ka	39%	0.605	±0.026	1.67	17%	4	25							
KK-31-100	Groundmass	Incremental Heating	Plateau	Excess Initial $^{40}Ar/^{36}Ar$ = 302.38 ± 0.34 (SD).	**87.3**	**±6.4 ka**	±6.7 ka	93%	0.821	±0.130	0.59	94%	23	25	87.1	±8.1 ka	±8.3 ka	302.39	± 0.68	0.65	88%
BN-07-100	Groundmass	Incremental Heating	Plateau		**188.5**	**±17.5 ka**	±18.0 ka	65%	0.123	±0.059	1.37	21%	8	25	177.1	±157.4 ka	±157.5 ka	296.52	±14.57	1.58	15%

					Inverse isochron								Total fusion				
Sample Name	Material	Experiment Type	Age Type	Notes	Age (ka)	±2σ (i)	±2σ (f)	$^{40}Ar/^{36}Ar$ intercept	±2σ	SF	MSWD	P	Age (ka)	±2σ (i)	±2σ (f)	K/Ca	±2σ
BU-01-100	Groundmass	Incremental Heating	Plateau														
BU-04-101	Groundmass	Incremental Heating	Plateau	Subatmospheric Initial $^{40}Ar/^{36}Ar = 294.00 \pm 2.35$ (SD).	20.8	±13.1 ka	±13.1 ka	297.21	±4.61	0%	1.36	19%	60.2	±15.2 ka	±15.3 ka	0.083	±0.000
BU-05-100	Groundmass	Incremental Heating	Mini Plateau		650.6	±78.7 ka	±80.1 ka	296.09	±2.86	15%	0.22	93%	765.7	±124.8 ka	±126.0 ka	0.028	±0.000
BU-06-100	Groundmass	Incremental Heating	Plateau	Excess Initial $^{40}Ar/^{36}Ar = 300.46 \pm 0.76$ (SD).	22.4	±1.7 ka	±1.8 ka	300.46	±1.52	13%	1.06	38%	1591.3	±52.3 ka	±63.5 ka	0.018	±0.000
BU-07-100	Groundmass	Incremental Heating	Plateau	Subatmospheric Initial $^{40}Ar/^{36}Ar = 288.92 \pm 3.14$ (SD).	129.2	±31.1 ka	±31.3 ka	288.02	±7.14	11%	2.53	0%	22.5	±1.5 ka	±1.6 ka	0.852	±0.001
BU-09-100	Groundmass	Incremental Heating	Plateau		27.6	±12.2 ka	±12.3 ka	296.77	±3.92	3%	2.59	0%	176.4	±18.7 ka	±19.1 ka	0.082	±0.000
BU-09-100	Biotite	Total Fusion	Ideogram										22.0	±1.3 ka	±1.4 ka	1.553	±0.003
BU-09-100	Biotite	Total Fusion	Total Fusion		57.9	±13.4 ka	±13.5 ka	295.48	±2.30	3%	0.85	70%	67.4	±12.4 ka	±12.5 ka	29.922	±5.858
BU-09-100	Biotite	Incremental Heating	Plateau		20.6	±1.6 ka	±1.6 ka	298.28	±4.03	26%	0.80	75%	297.1	±109.3 ka	±109.5 ka	−8.592	±6.392
BU-11-100	Groundmass	Incremental Heating	Plateau	Excess Initial $^{40}Ar/^{36}Ar = 298.37 \pm 2.04$ (SD).	20.9	±4.0 ka	±4.1 ka	298.37	±4.08	11%	0.18	100%	59.4	±5.3 ka	±5.5 ka	60.841	±12.544
BU-11-100	Plagioclase	Incremental Heating	Plateau	Excess Initial $^{40}Ar/^{36}Ar = 402.18 \pm 32.62$ (SD).	11.4	±5.5 ka	±5.5 ka	402.18	±65.25	7%	1.85	2%	20.9	±2.6 ka	±2.7 ka	1.769	±0.003
BUM-01	Groundmass	Incremental Heating	Plateau										11.8	±11.6 ka	±11.6 ka	0.093	±0.000
BUR-01	Groundmass	Incremental Heating	Mini Plateau										1336.7	±107.0 ka	±111.2 ka	0.032	±0.000
KK-31-100	Groundmass	Incremental Heating	Plateau	Excess Initial $^{40}Ar/^{36}Ar = 302.38 \pm 0.34$ (SD).	87.4	±7.9 ka	±8.2 ka	302.38	±0.68	7%	0.64	89%	107.1	±18.4 ka	±18.5 ka	0.352	±0.001
BN-07-100	Groundmass	Incremental Heating	Plateau		177.3	±104.2 ka	±104.3 ka	296.55	±14.73	2%	1.59	14%	910.8	±46.2 ka	±50.6 ka	0.165	±0.001

Table 3
Representative olivine and clinopyroxene compositions from primitive, highly magnesian samples (BU-04-100 and BU-06-100) and more evolved, less magnesian samples (BU-08-100 and BU-11-100) used in least-squares mixing calculations.

Sample	SiO_2	TiO_2	Al_2O_3	Cr_2O_3	FeO	MnO	MgO	CaO	Na_2O	K_2O	P_2O_5	Mg#
Clinopyroxene												
BU-04-100 pyx3 core	38.95	2.69	7.17	0.01	9.59	0.17	9.50	20.81	0.95	0.01	1.50	64
BU-06-100 pyx4 core	45.87	1.04	3.89	0.37	4.44	0.09	15.43	20.53	0.45	0.01	1.66	86
BU-06-100 pyx1	42.46	1.80	4.81	0.30	6.16	0.14	13.25	20.52	0.35	0.01	1.50	79
BU-11-100 pyx5	48.34	1.92	4.07	0.02	9.39	0.19	13.91	20.78	0.39	0.00	0.00	73
Olivine												
BU-04-100 ol2 core	38.17	0.01	0.04	0.03	11.85	0.18	47.65	0.32	0.01	0.00	1.74	88
BU-06-100 ol2	39.76	0.00	0.05	0.03	14.28	0.20	45.34	0.31	0.01	0.02	0.00	85
BU-08-100 ol1	37.39	0.02	0.03	0.00	21.98	0.33	40.02	0.22	0.01	0.00	0.00	76
BU-11-100 ol7 core	35.78	0.04	0.02	0.01	30.17	0.44	33.22	0.32	0.00	0.00	0.00	66

also elevated above primitive mantle (~2.6; Kramers and Tolstikhin, 1997) in both sample suites (4–10 in most Bufumbira and Toro Ankole samples), another proxy for residual garnet. The Toro Ankole samples also have higher CaO/Al_2O_3 (0.87–3.03; 0.31–1.34 at Bufumbira), further supporting a garnet-bearing source.

Lavas from both provinces display evidence for hydrous phases in their source lithosphere, though the distribution of phlogopite and amphibole in the lithospheric source region remains imperfectly resolved. Both hydrous mafic minerals can grow in veins within previously depleted mantle lithologies in response to the infiltration of metasomatic magmas or fluids. Bufumbira lavas generally have Rb/Sr elevated above primitive mantle, suggestive of source phlogopite (Adam et al., 1993; LaTourrette et al., 1995), while Toro Ankole samples have low Rb/Sr with elevated Ba/Rb, indicating the presence of amphibole (Fig. 8); we infer the presence of phlogopite beneath Toro Ankole as well, as these lavas have extremely high K_2O contents and their associated xenoliths contain phlogopite. Amphibole is supported in the lithosphere beneath Toro Ankole by elevated Sm/Hf and Sm/Zr in the erupted lavas; these ratios are elevated in Toro Ankole samples but form a continuous range with Bufumbira lavas (Fig. 8). Another potential signature of source amphibole, Zr/Nb, is elevated in Bufumbira lavas though not in the Toro Ankole lavas (Fig. 8). K/Rb, generally <400 in phlogopite and >1100 for melts derived from amphibole-bearing sources (Basu, 1978; Beswick, 1976), is relatively low for Bufumbira (90–578) and Katwe-Kikorongo and Bunyaruguru (128–423), suggestive of phlogopite but permissive of other alternatives including amphibole. K/Rb values of 231–356 and elevated LREE/HREE at Nyamuragira and Nyiragongo indicate that phlogopite and garnet are also important source minerals elsewhere in the Virunga province (Chakrabarti et al., 2009a).

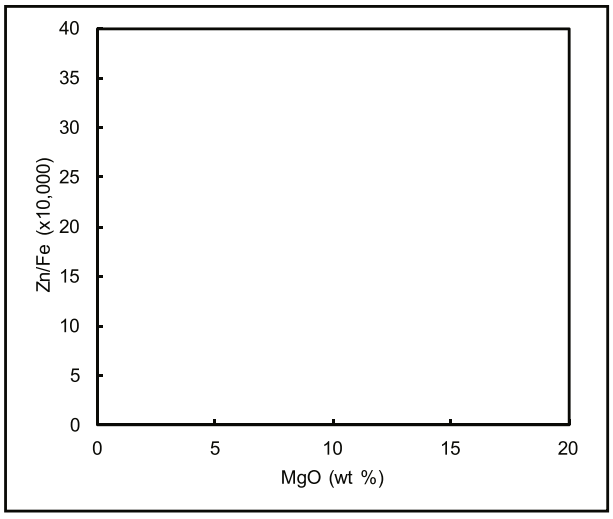

Fig. 7. Zn/Fe ($x10^4$) for most Bufumbira and Katwe-Kikorongo samples are slightly elevated above typical values for melts originating from peridotite (~8–10; shaded bar), suggesting a pyroxenitic source for these lavas (Le Roux et al., 2010, 2011). Karisimbi PKBs show slightly lower values.

Accessory amounts of apatite, titanite, and zircon also play a role in the trace element systematics of these lavas. Apatite is common in lithospheric mantle following metasomatism, particularly if carbonatitic fluids are involved. Apatite in the source of Toro Ankole lavas may produce the elevated Th and U in those lavas, as well as contributing to their extreme LREE/HREE enrichments (Chazot et al., 1996). The presence of minor refractory zircon in the Toro Ankole source region could explain the low Zr/Nb there, which would otherwise be expected to be higher given other indicators of amphibole.

5.3.2. Depth and conditions of melting

Like many other examples of continental alkaline magmatism, Bufumbira and Katwe-Kikorongo lavas are likely products of low degrees of partial melting. The moderately high $(La/Yb)_n$ of Bufumbira mafic lavas is consistent with this interpretation. Steep REE profiles and very high $(La/Yb)_n$ ratios (68–133) of Toro Ankole lavas may be a result of exceptionally low degrees of melting, suggested by the high proportion of network modifying elements K and P that reduce melt viscosity and enhance transport and eruptability. The difference in $(Tb/Yb)_n$ between the two provinces is primarily controlled by lower Yb concentrations in Toro Ankole lavas, consistent with smaller degree of melting.

Bulk compositions of primitive Bufumbira lavas and PKBs plot between the experimentally-determined 1 bar and 8–30 kbar (0.8–3 GPa) cotectics of Sack et al. (1987) and show trends consistent with fractionation of olivine and olivine + pyroxene following equilibration at the deeper cotectic (Fig. 9). This expression suggests that the lavas erupted rapidly from depths of ~25+ km, consistent with a lack of evidence for extensive shallow fractionation and crustal contamination, though an apparent underestimate given the inferred presence of garnet in the source. Katwe-Kikorongo lavas do not plot within the experimental cotectics in Fig. 9a and thus their depths of origin cannot be reliably determined from these diagrams.

Thermobarometry places additional constraints on the conditions of formation of the primitive lavas from Bufumbira; the undersaturated compositions of Katwe-Kikorongo lavas do not yield successful results with any of the methods described here. We used the thermobarometer of Lee et al. (2009), based on bulk rock composition, to determine temperatures and pressures of melting for the Bufumbira lavas. This method is based on experimental data on melts from olivine + orthopyroxene bearing sources and is thus not ideal for the compositions inferred for the Western Rift, nor for silica-undersaturated melt compositions. We restrict our use of this approach to Bufumbira lavas with $SiO_2 > 43\%$ and MgO > 7.8 wt% and view the results with caution. Bufumbira lavas are calculated to have equilibrated at 2.2–5.0 GPa (~65–150 km)

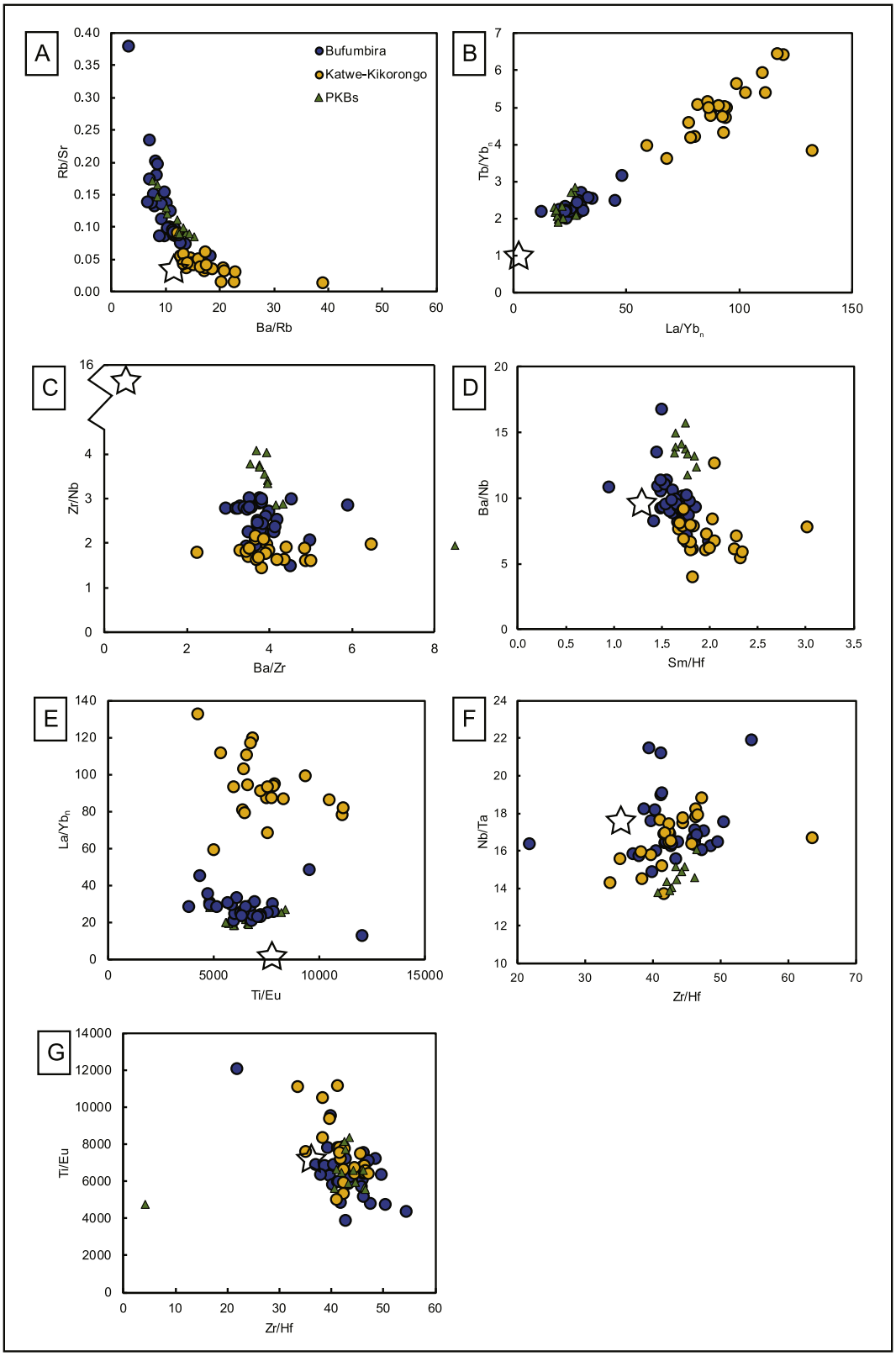

Fig. 8. Trace element differences between Katwe-Kikorongo and Bufumbira are subtle but provide important constraints on source mineralogy. Primitive mantle values from Sun and McDonough (1989) shown with stars. A) Chondrite-normalized Tb/Yb values suggest abundant garnet in the source material for Toro Ankole magmas; values observed at Bufumbira may reflect minor garnet in combination with HREE control by clinopyroxene at depths near the spinel-garnet transition (Blundy et al., 1998). B) Our lavas show different patterns of metasomatism in the magmatic source region: in Bufumbira elevated Rb/Sr suggests the presence of phlogopite, while in Toro Ankole elevated Ba/Rb suggests amphibole. C) Conversely, elevated Zr/Nb in Virunga lavas argues for the presence of amphibole there, while D) Sm/Hf, elevated above mantle values in both locations, argues for the presence of amphibole in both areas. E) and F) Ti/Eu, Nb/Ta, and Zr/Hf are all elevated over values associated with melting of anhydrous peridotite, further evidence for metasomatic enrichment of the lithosphere beneath Toro Ankole and Virunga.

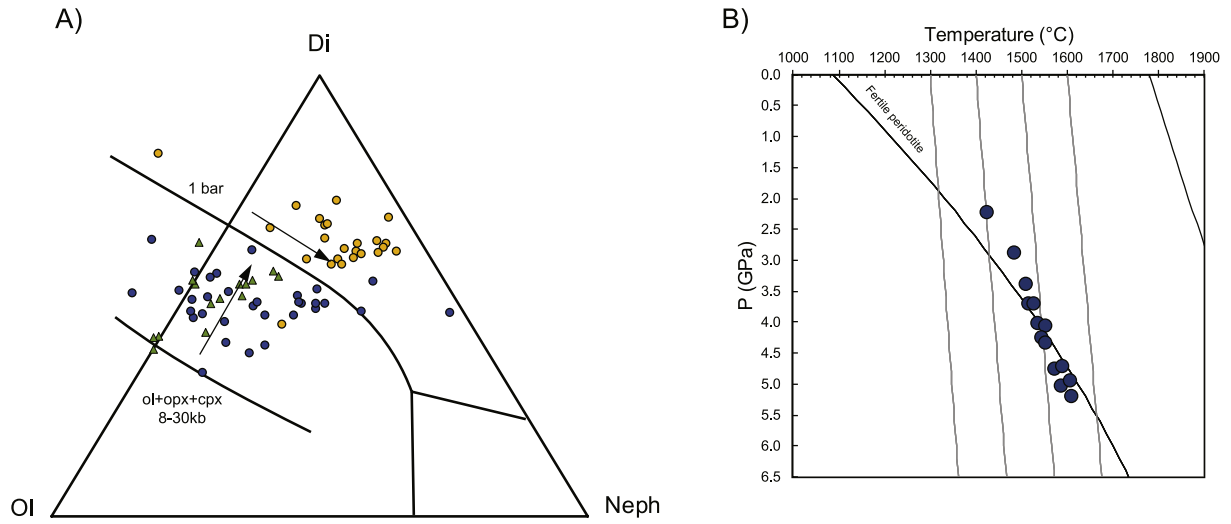

Fig. 9. Geothermobarometry of Western Rift lavas. (A) Bufumbira and Katwe-Kikorongo samples (this study) and Karisimbi PKBs (Rogers et al., 1998) plot between the 1 bar and 8–30 kbar experimental cotectics of Sack et al. (1987) in the diopside-olivine-nepheline pseudoternary and show trends consistent with fractionation of olivine and olivine + pyroxene following equilibration at the deeper cotectic. Katwe-Kikorongo lavas fall outside the cotectics and do not fit within this framework. (B) T and P of melt segregation from mantle calculated from Lee et al. (2009) thermobarometer, with fertile peridotite solidus of (Hirschmann, 2000).

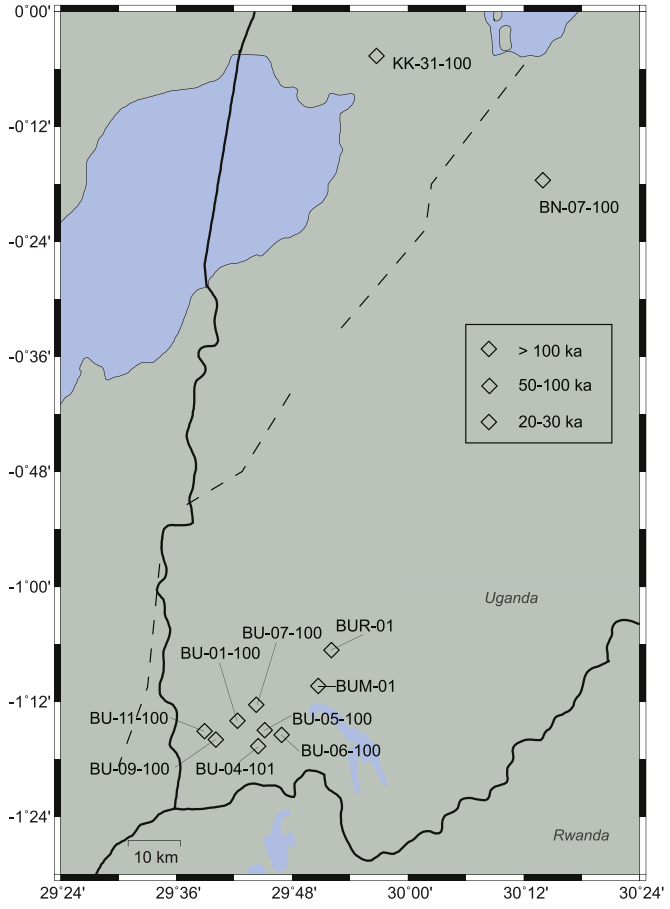

Fig. 10. Map of locations of samples dated with argon dating. Purple diamonds: >100 ka, green diamonds: 50–100 ka, gray diamonds: 20–30 ka. Dashed lines indicate approximate locations of eastern rift-bounding faults for the Western Rift; additional smaller faults are present throughout Bufumbira. (For interpretation of the references to colour in this figure legend, the reader is referred to the web version of this article.)

and T_p ~ 1400–1550, defining a geotherm with a steeper slope than the dry peridotite solidus (Fig. 9b). The deepest melts equilibrated below the dry peridotite solidus, indicating that a source with volatiles is required. For Katwe-Kikorongo lavas, calculated pressures exceed the calibrated range of the method (i.e. >8 GPa) and the source region appears to be dominated by non-peridotite materials. We note, however, that the P and T predicted by the method for the Katwe-Kikorongo lavas are high, suggesting deeper melting in the presence of volatiles at hotter temperatures relative to Bufumbira, consistent with the model of Rosenthal et al. (2009) and the REE systematics discussed above.

The thermobarometers of Putirka et al. (1996) and Neave and Putirka (2017), which employ clinopyroxene chemistry and clinopyroxene-liquid equilibrium, were also used to calculate equilibration depths and pressures for these lavas. Clinopyroxene thermobarometry for these lavas (Pitcavage, 2020) found pressures of equilibration for phenocryst cores in Bufumbira lavas reach a maximum of 1.5 GPa (50 km). Clinopyroxene phenocrysts in equilibrium with their host lavas equilibrated at temperatures of ~1200–1250 °C. This pressure is significantly less than the results of the bulk rock barometers discussed above; it is likely that the clinopyroxene phenocrysts did not form shortly after melt separation but equilibrated following a period of ascent.

Broader geochemical and geophysical evidence throughout the Western Rift suggests that the depth of melting varies along the rift axis, potentially providing an explanation for some of the trace element variability between the two provinces. We concur with the general conclusions of Rosenthal et al. (2009), who argued for an increase in lithospheric thickness and in depth of melting from south to north to explain differences in magmatic chemistry between Kivu, Virunga, and Toro Ankole. Receiver function analysis in Toro Ankole found crustal thickness of ~30 km in the rift valley (Wölbern et al., 2010), with regions of potential melt present to depths of at least 70 km; basin-bounding border faults may penetrate up to 20 km in Virunga (Ebinger, 1989). This is consistent with the bulk rock geobarometers as well as with the presence of phlogopite-bearing xenoliths and REE systematics requiring the presence of residual garnet in the sources for Toro Ankole (and possibly Bufumbira), suggesting that hydrous lithospheric material is contributing to melts at depths of 70–90 km depth. Meanwhile,

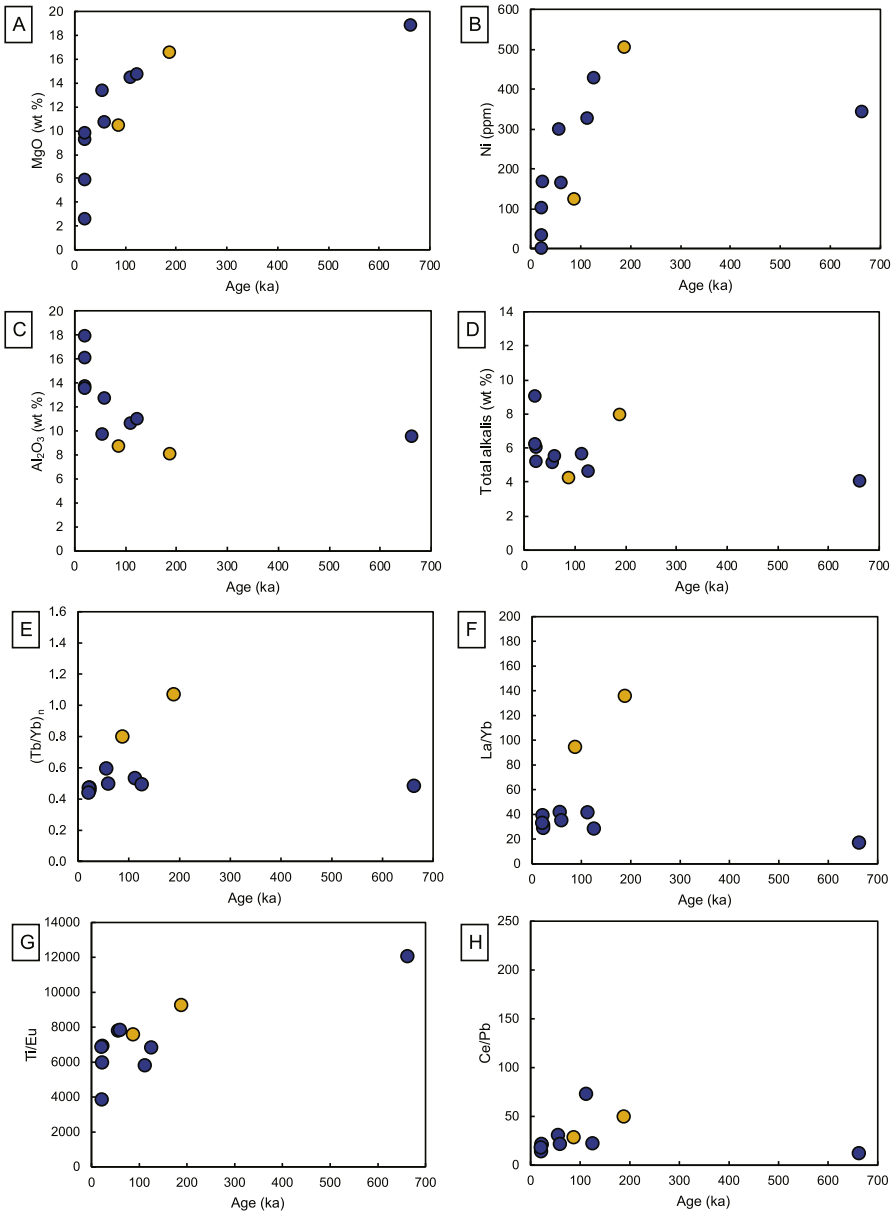

Fig. 11. Variations in some major and minor elements (A–D) with age suggest that temporal controls on magma compositions are related to fractionation. Trace element indicators of extent and depth of melting, metasomatism, and crustal contamination (E–H) do not vary systematically with age, suggesting that fundamental source properties of these magmas are not varying significantly over time.

geochemical signatures of slightly shallower (~65 km) melting are observed for the Kivu volcanic province (Furman and Graham, 1999).

5.3.3. Metasomatic history

While primitive lavas from both provinces have overall high abundances of incompatible trace elements, there are fundamental differences in the degree and style of enrichment between Katwe-Kikorongo and Bufumbira (Figs. 4, 5, 6, 8). The mineralogy of the source material, discussed above, is consistent with a history of mantle metasomatism in the regional lithosphere. The mineralogy of lithospheric mantle can be modified by growth of metasomatic phases concurrent with infiltration of melts and fluids; the trace element signatures of these metasomatic minerals can be diagnostic of the type of metasomatic agent involved. We focus here on determining metasomatic agents through identification of the source phase assemblages sampled by mafic volcanism in each area.

Primitive alkaline lavas from both volcanic provinces record the presence of metasomatic mineralogy in their source material. Toro Ankole lavas appear to be derived from a pyroxenitic source with clinopyroxene + amphibole ± phlogopite ± garnet ± apatite ± titanite, while the Bufumbira lavas from Virunga are consistent with clinopyroxene ± amphibole ± phlogopite. These compositions demonstrate that ancient sub-continental lithospheric mantle (likely previously melt-depleted harzburgite or lherzolite) was enriched by metasomatic fluids and/or melts prior to Cenozoic EARS magmatism in the Western Rift. The trace element compositions of the lavas vary over short spatial scales, implying heterogeneity in the degree and/or style of metasomatic enrichment within each volcanic field. This heterogeneity may exist vertically as well as laterally, though any consideration of vertical variability in metasomatic compositions must account for the presence of phlogopite and garnet in the source material and the depths suggested by their presence, as discussed above.

To first order, the geochemical signatures of mafic lavas from the northern Western Rift can be attributed to modification of the mantle source by both carbonatitic and low-degree silicate melts. We note that the relationship between deep carbonated-silicate melts acting as metasomatic agents and extruded carbonatite lavas is enigmatic (Tappe et al., 2017). We therefore interpret the trace element signatures of carbonate-rich metasomatism with caution, as carbonatitic tuffs are present within Toro Ankole (Barker and Nixon, 1989; Nixon, 1967); however, it is apparent that carbonate material is playing some role in mantle modification.

Among Katwe-Kikorongo lavas, high CaO is correlated with low SiO_2, a signature of melts of carbonated peridotite (Dasgupta et al., 2007). High Ba/Rb values in these lavas indicating abundant amphibole in the source is also consistent with a carbon-rich metasomatic agent. Bufumbira and Katwe-Kikorongo lavas have overlapping Zr/Hf (22–64) values that extend from near primitive mantle values to pronounced Zr enrichment. Such HFSE enrichment has been associated with growth of amphibole, potentially along with clinopyroxene, phlogopite and/or titanite in response to movement of carbonatites through the lithosphere (Chakhmouradian, 2006; Dupuy et al., 1992). Katwe-Kikorongo shows weak correlation between Zr/Hf and Nb/Ta (Fig. 8); these ratios approach values expected for carbonatites (Chakhmouradian, 2006), but do not preclude silicate metasomatic agents. Elevated La/Yb_n values in Katwe-Kikorongo mafic lavas are similar to observations from xenoliths following carbonatitic metasomatism (Coltorti et al., 1999).

Relative to the effects of carbonatitic metasomatism, silicate-dominated metasomatism typically produces mantle material with less extreme REE enrichment coupled with less extreme depletion in Ti, Zr and Sr (Klemme et al., 1995; Rudnick et al., 1993). Bufumbira and Katwe-Kikorongo lavas have similar ranges of Ti/Eu (3800–12,000) that are elevated over melts derived from anhydrous peridotite, and are recognized as signatures of silicate, rather than carbonatitic, metasomatism (Coltorti et al., 1999; Rudnick et al., 1993).

We interpret these geochemical signatures collectively to reflect an episode of carbonatitic metasomatism in both provinces, with additional silicate metasomatism at Bufumbira. The evidence for carbonated lithospheric mantle at depth is stronger for the Toro Ankole samples, but cannot be ruled out in Virunga. Carbon can be concentrated along cratonic margins as it becomes remobilized during tectonic events (Foley and Fischer, 2017). As there is cratonic crust close to Toro Ankole, there is a greater signature of carbon remobilized from cratonic mantle in the source of the lavas. We suggest that low degree melts of such a deep carbonated lithospheric mantle dominate in Toro Ankole, while Virunga primitive magmas represent melts from slightly shallower portions of the lithosphere, where the lithosphere is thinner and silicate melts from Proterozoic mobile belt material dominates. The differing prevalence of silicate and carbonatitic metasomatic agents may explain much of the observed compositional variability in the region, though local metasomatic heterogeneities on a km-scale exist within each province.

We conclude that a minimum of two distinct metasomatic events are required for the northern provinces of the Western Rift. Rosenthal et al. (2009) suggested that the mafic lavas of Toro Ankole provide geochemical evidence for two metasomatic events beneath that province: the first resulting in a phlogopite-rich, MARID-like assemblage, and a later carbonate-rich metasomatic fluid. Separately, (Hudgins et al., 2015) demonstrated that melt inclusions from Bufumbira lavas had high CO_2 and H_2O contents, as well as Li/Yb and B/Be ratios indicative of metasomatism by subduction-related fluids. We suggest that subduction-related geochemical modification was limited to fluids, as we find no evidence for direct input from melted sediments, e.g., relative to the global subducting sediments of GLOSS II (Plank, 2014), the bulk rock compositions for the Katwe-Kikorongo and Bufumbira lavas are moderately enriched in Nb, Ta, Ti, and LREE-MREE, and depleted in Pb and HREE (Supplementary information). The timing of this event is not constrained by our new data, though it is geologically reasonable that a subduction signature is could be associated with late Pan-African subduction, and is consistent with Pb and Sr isotopic data (~500 Ma) that were interpreted as a manifestation of that event (Vollmer and Norry, 1983).

5.3.4. Structural and tectonic controls on magmatism

We conclude from observed variability in trace element compositions that the regional SCLM in the northern provinces of the Western Rift is heterogeneous in composition and/or melting conditions over geologically short spatial scales (<2 km). The oldest and most primitive Bufumbira samples define a NW-SE trending cluster of cones within the central portion of the field, parallel to the strike of faults and fractures in the volcanic field (e.g. Pouclet et al., 2016; Fig. 10). These faults are not parallel to the major rift-bounding faults and mirror instead the structural fabric of the metamorphic basement that comprises the mobile belt.

Younger lavas on either side of the central cluster (Fig. 10) are geochemically distinct from the older cones and from one another. Samples BUM-01 and BUR-01 come from east of the main Bufumbira field away from the rift axis. Both samples are primitive alkaline lavas (MgO 10–14 wt%) and their incompatible trace element abundances are among the lowest in the suite. Lavas from the southwestern portion of Bufumbira (closer to the large Virunga volcanoes) are generally higher in SiO_2 and alkalis and lower in MgO and are classified as K-hawaiites and K-mugearites, and are generally younger than the most primitive lavas, located in the east-central portion of the volcanic field (Fig. 10).

The differences in metasomatic history that drive the geochemical variability in the northern Western Rift can be traced to their geologic history. The Toro Ankole and Virunga Volcanic Provinces are situated where Proterozoic mobile belts meet the Tanzanian Craton, but Toro Ankole straddles a region where a lithospheric link between the Tanzanian and Congo cratons is inferred from geophysical evidence (Link et al., 2010; Wölbern et al., 2010). Our assessment of primitive lavas from both provinces indicates that melting beneath Toro Ankole is occurring deeper and in thicker lithosphere.

This petrogenetic model has important implications for our understanding of the geodynamics of the northern Western Rift. Melting of deep carbonated lithospheric material, containing hydrous metasomatic minerals, does not require the high mantle potential temperatures of asthenospheric upwelling characteristic of the Afar region of the EARS. The constraints on melting conditions and metasomatic mineralogy we describe above provide important information that can in turn inform our regional understanding of Western Rift magmatism. As discussed previously, magmas are derived from progressively shallower depths in the lithosphere from north to south within the Western Rift. We emphasize that a combination of factors from progressively thinning lithosphere, variably fusible metasomes, and the presence of remobilized cratonic carbonate produce this change in melting depth, as well as the variations in major, trace element and isotope geochemistry that are observed within the Western Rift.

Magmatic compositions similarly indicative of similarly deep lithospheric melting have been observed in other portions of the EARS (Mana et al., 2012; (Paslick et al., 1995). In particular, the northern portion of the Western Rift shares characteristics with the Northern Tanzania Divergence (NTD), where melts of metasomatized lithospheric mantle with residual garnet and phlogopite have been identified (e.g. Mana et al., 2012). Similar to Virunga and Toro Ankole, the NTD is in the early stages of rift development in a zone of pre-existing lithospheric weakness along the margin of the Tanzanian Craton (e.g. Le Gall et al., 2008). NTD lavas are isotopically distinct from much of the Western Rift, suggesting that while similar processes are occurring in the two regions, magmas may be sampling lithospheric mantle modified at different times (Mana et al., 2012). Metasomatized lithospheric mantle was also identified as an important source component in the

Gerba Guracha volcanics of Ethiopia (Rooney et al., 2014), representing a source distinct from the Afar mantle plume. Low-degree partial melts of metasomatized lithospheric mantle, as observed in these EARS locales, demonstrate that magmatism can occur without significant mantle plume input or high temperatures, and that such magmatism may be especially important in young, developing portions of a rift system such as the Western Rift or NTD.

6. Conclusions

Major and trace element geochemistry of primitive lavas from three primitive volcanic fields—Bufumbira, and Katwe-Kikorongo and Bunyaruguru—located in the Virunga and Toro Ankole Volcanic Provinces, respectively, were used to probe the variation and controls on the petrogenesis of magmas in the northern portion of the Western Rift. The lavas were dated to ages of 21–662 ka, with shifts in major and minor element compositions observed over time.

While the two provinces have broad compositional similarities, fundamental differences in trace element enrichment are observed. The source material for these magmas is dominated by contributions from metasomatized lithospheric mantle. The mineralogy of metasomatically enriched lithosphere varies between the two volcanic provinces, despite their relatively close geographic association; local variability within each volcanic field and province is also evident. Bulk-rock thermobarometry, trace element enrichment, and least-squares mixing calculations are consistent with minor fractionation control on magma compositions and indicate that repeated small volume melts were derived from depth within the lithospheric mantle.

Supplementary data to this article can be found online at https://doi.org/10.1016/j.lithos.2021.106192.

Declaration of Competing Interest

The authors declare that they have no known competing financial interests or personal relationships that could have appeared to influence the work reported in this paper.

Acknowledgements

We gratefully acknowledge funding from the Ohmoto, Knopf, Leblanc, Voight, Standish Good, and Krynine Scholarships through Penn State University. Portions of this work were funded by NSF EAR1753696 to Furman and Nelson. Many thanks to Melanie Saffer, Henry Gong, and Matt Gonzales (Penn State) and Anthony Koppers and Dan Miggins (Oregon State University) for analytical assistance. We thank two anonymous reviewers and editor Michael Roden for insightful and constructive comments that improved the manuscript.

References

Adam, J., Green, T.H., Sie, S.H., 1993. Proton microprobe determined partitioning of Rb, Sr, Ba, Y, Zr, Nb and Ta between experimentally produced amphiboles and silicate melts with variable F content. Chem. Geol. 109, 29–49.

Aoki, K.-I., Yoshida, T., Nakamura, Y., 1985. Petrology and Geochemistry of the Nyamuragira Volcano, Zaire. Journal of Volcanology and Geothermal Research 25, 1–28.

Baker, J.A., Thirlwall, M.F., Menzies, M.A., 1996. Sr-Nd-Pb isotopic and trace element evidence for crustal contamination of plume-derived flood basalts: oligocene flood volcanism in western Yemen. Geochim. Cosmochim. Acta 60, 2559–2581. https://doi.org/10.1016/0016-7037(96)00105-6.

Barker, D.S., Nixon, P.H., 1989. High-Ca, low-alkali carbonatite volcanism at Fort Portal, Uganda. Contrib. Mineral. Petrol. 103, 166–177. https://doi.org/10.1007/BF00378502.

Basu, A.R., 1978. Trace elements and Sr-isotopes in some mantle-derived hydrous minerals and their significance. Geochim. Cosmochim. Acta 42, 659–668.

Begg, G.C., Griffin, W.L., Natapov, L.M., O'Reilly, S.Y., Grand, S.P., O'Neill, C.J., Hronsky, J.M.A., Djomani, Y.P., Swain, C.J., Deen, T., Bowden, P., 2009. The lithospheric architecture of Africa: Seismic tomography, mantle petrology, and tectonic evolution. Geosphere 5, 23–50. https://doi.org/10.1130/GES00179.1.

Beswick, A.E., 1976. K and Rb relations in basalts and other mantle derived materials. Is phlogopite the key? Geochim. Cosmochim. Acta 40, 1167–1183. https://doi.org/10.1016/0016-7037(76)90152-6.

Blundy, J.D., Robinson, J.A.C., Wood, B.J., 1998. Heavy REE are compatible in clinopyroxene on the spinel lherzolite solidus. Earth Planet. Sci. Lett. 160, 493–504.

Boven, A., Pasteels, P., Punzalan, L.E., Yamba, T.K., Musisi, J.H., 1998. Quaternary perpotassic magmatism in Uganda (Toro-Ankole Volcanic Province): age assessment and significance for magmatic evolution along the East African Rift. J. Afr. Earth Sci. 26, 463–476.

Bryan, W.B., Finger, L.W., Chayes, F., 1969. Estimating proportions in petrographic mixing equations by least-squares approximation. Science 163 (80), 926–927.

Carr, M.J., Gazel, E., 2017. Igpet software for modeling igneous processes: examples of application using the open educational version. Mineral. Petrol. 111, 283–289. https://doi.org/10.1007/s00710-016-0473-z.

Chakhmouradian, A.R., 2006. High-field-strength elements in carbonatitic rocks: geochemistry, crystal chemistry and significance for constraining the sources of carbonatites. Chem. Geol. 235, 138–160. https://doi.org/10.1016/j.chemgeo.2006.06.008.

Chakrabarti, R., Basu, A.R., Santo, A.P., Tedesco, D., Vaselli, O., 2009a. Isotopic and geochemical evidence for a heterogeneous mantle plume origin of the Virunga volcanics, Western rift, East African Rift system. Chem. Geol. 259, 273–289. https://doi.org/10.1016/j.chemgeo.2008.11.010.

Chakrabarti, R., Sims, K.W.W., Basu, A.R., Reagan, M., Durieux, J., 2009b. Timescales of magmatic processes and eruption ages of the Nyiragongo volcanics from 238U-230Th-226Ra-210Pb disequilibria. Earth Planet. Sci. Lett. 288, 149–157. https://doi.org/10.1016/j.epsl.2009.09.017.

Chazot, G., Menzies, M.A., Harte, B., 1996. Determination of partition coefficients between apatite, clinopyroxene, amphibole, and melt in natural spinel lherzolites from Yemen: implications for wet melting of the lithospheric mantle. Geochim. Cosmochim. Acta 60, 423–437. https://doi.org/10.1016/0016-7037(95)00412-2.

Chorowicz, J., 2005. The East African rift system. J. Afr. Earth Sci. 43, 379–410. https://doi.org/10.1016/j.jafrearsci.2005.07.019.

Coltorti, M., Bonadiman, C., Hinton, R.W., Siena, F., Upton, B.G.J., 1999. Carbonatite metasomatism of the oceanic upper mantle: evidence from clinopyroxenes and glasses in ultramafic xenoliths of Grande Comore, Indian Ocean. J. Petrol. 40, 133–165. https://doi.org/10.1093/petroj/40.1.133.

Cox, K.G., Bell, J.D., Pankhurst, J., 1979. The Interpretation of Igneous Rocks. Springer.

Dasgupta, R., Hirschmann, M.M., Smith, N.D., 2007. Partial melting experiments of peridotite + CO2 at 3 GPa and genesis of alkalic ocean island basalts. J. Petrol. 48, 2093–2124. https://doi.org/10.1093/petrology/egm053.

Davies, G.R., Lloyd, F.E., 1989. Pb-Sr-Nd isotope and trace element data bearing on the origin of the potassic subcontinental lithosphere beneath south-west Uganda. Kimberlites Relat. Rocks 2, 784–794.

Dawson, J.B., Smith, J.V., 1977. The MARID (mica-amphibole-rutile-ilmenite-diopside) suite of xenoliths in kimberlite. Geochim. Cosmochim. Acta 41, 309–323.

De Mulder, M., Pasteels, P., 1986. K-Ar geochronology of the Karisimbi volcano (Virunga, Rwanda-Zaire). J. Afr. Earth Sci. 5, 575–579. https://doi.org/10.1016/0899-5362(86)90023-0.

De Mulder, M., Hertogen, J., Deutsch, S., André, L., 1986. The role of crustal contamination in the potassic suite of the Karisimbi Volcano (Virunga, African Rift Valley). Chem. Geol. 57, 117–136. https://doi.org/10.1016/0009-2541(86)90097-5.

Dupuy, C., Liotard, J.M., Dostal, J., 1992. Zr/Hf fractionation in intraplate basaltic rocks: Carbonate metasomatism in the mantle source. Geochim. Cosmochim. Acta 56, 2417–2423. https://doi.org/10.1016/0016-7037(92)90198-R.

Ebinger, C.J., 1989. Geometric and kinematic development of border faults and accomodation zones, Kivu-Rusizi Rift, Africa. Tectonics 8, 117–133.

Ebinger, C.J., Yemane, T., Woldegabriel, G., Aronson, J.L., Walter, R.C., 1993. Late Eocene-recent volcanism and faulting in the southern main Ethiopian rift. J. Geol. Soc. 150, 99–108. https://doi.org/10.1144/gsjgs.150.1.0099.

Ebinger, C.J., Yemane, T., Harding, D.J., Tesfaye, S., Kelley, S., Rex, D.C., 2000. Rift deflection, migration, and propagation: linkage of the Ethiopian and Eastern rifts, Africa. GSA Bull. 112, 163–176.

Emry, E.L., Shen, Y., Nyblade, A.A., Flinders, A., Bao, X., 2018. Upper mantle earth structure in Africa from full-wave ambient noise tomography. Geochem. Geophys. Geosyst. 20, 120–147. https://doi.org/10.1029/2018GC007804.

Foley, S.F., Fischer, T.P., 2017. An essential role for continental rifts and lithosphere in the deep carbon cycle. Nat. Geosci. 10, 897–902. https://doi.org/10.1038/s41561-017-0002-7.

Furman, T., 1995. Melting of metasomatized subcontinental lithosphere: undersaturated mafic lavas from Rungwe, Tanzania. Contrib. Mineral. Petrol. 122, 97–115.

Furman, T., Graham, D., 1999. Erosion of lithospheric mantle beneath the East African Rift system: geochemical evidence from the Kivu volcanic province. Lithos 48, 237–262. https://doi.org/10.1016/S0024-4937(99)00031-6.

George, R., Rogers, N., Kelley, S., 1998. Earliest magmatism in Ethiopia: evidence for two mantle plumes in one flood basalt province. Geology 26, 923–926.

Hirschmann, M.M., 2000. Mantle solidus: Experimental constraints and the effects of peridotite composition. Geochemistry, Geophysics, Geosystems 1.

Hofmann, A.W., Jochum, K.P., Seufert, M., White, W.M., 1986. Nb and Pb in oceanic basalts: new constraints on mantle evolution. Earth Planet. Sci. Lett. 79, 33–45. https://doi.org/10.1016/0012-821X(86)90038-5.

Holmes, A., Harwood, H.F., 1932. Petrology of the volcanic fields east and south-east of Ruwenzori, Uganda. Q. J. Geol. Soc. 88, 370–442. https://doi.org/10.1144/GSL.JGS.1932.088.01-04.16.

Holmes, A., Harwood, H.F., 1937. The Volcanic Area of Bufumbira, Geologic Survey of Uganda. Geologic Survey of Uganda.

Hudgins, Thomas R., Mukasa, S.B., Simon, A.C., Moore, G., Barifaijo, E., 2015. Melt inclusion evidence for CO_2-rich melts beneath the western branch of the East African Rift: implications for long-term storage of volatiles in the deep lithospheric mantle. Contributions to Mineralogy and Petrology 169.

Johnson, M.C., Plank, T., 2000. Dehydration and melting experiments constrain the fate of subducted sediments. Geochem. Geophys. Geosyst. 1. https://doi.org/10.1029/1999GC000014.

Kampunzu, A.B., Bonhomme, M.G., Kanika, M., 1998. Geochronology of volcanic rocks and evolution of the Cenozoic western branch of the East African Rift system. J. Afr. Earth Sci. 26, 441–461. https://doi.org/10.1016/S0899-5362(98)00025-6.

Kelley, K.A., Plank, T., Ludden, J., Staudigel, H., 2003. Composition of altered oceanic crust at ODP Sites 801 and 1149. Geochem. Geophys. Geosyst. 4. https://doi.org/10.1029/2002GC000435.

Klemme, S., van der Laan, S.R., Foley, S.F., Gunther, D., 1995. Experimentally determined trace and minor element partitioning between clinopyroxene and carbonatite melt under upper mantle conditions. Earth Planet. Sci. Lett. 133, 439–448. https://doi.org/10.1016/0012-821X(95)00098-W.

Konrad, K., Koppers, A.A.P., Balbas, A.M., Miggins, D.P., Heaton, D.E., 2019. Dating clinopyroxene phenocrysts in submarine basalts using 40Ar/39Ar geochronology. Geochem. Geophys. Geosyst. 20, 1041–1053. https://doi.org/10.1029/2018GC007697.

Koppers, A.A.P., 2002. ArArCALC software for 40Ar/39Ar age calculations. Comput. Geosci. 28, 605–619.

Koppers, A.A.P., Staudigel, H., Wijbrans, J.R., 2000. Dating crystalline groundmass separates of altered Cretaceous seamount basalts by the 40Ar/39Ar incremental heating technique. Chem. Geol. 166, 139–158. https://doi.org/10.1016/S0009-2541(99)00188-6.

Kramers, J.D., Tolstikhin, I.N., 1997. Two terrestrial lead isotope paradoxes, forward transport modelling, core formation and the history of the continental crust. Chemical 139, 75–110.

Kuiper, K.F., Deino, A., Hilgen, F.J., Krijgsman, W., Renne, P.R., Wijbrans, J.R., 2008. Synchronizing Rock Clocks of Earth History. Science 320, 500–504.

LaTourrette, T., Hervig, R.L., Holloway, J.R., 1995. Trace element partitioning between amphibole, phlogopite, and basanite melt. Earth Planet. Sci. Lett. 135, 13–30.

Le Gall, B., Nonnotte, P., Rolet, J., Benoit, M., Guillou, H., Mousseau-Nonnotte, M., Albaric, J., Deverchère, J., 2008. Rift propagation at craton margin. Distribution of faulting and volcanism in the North Tanzanian Divergence (East Africa) during Neogene times. Tectonophysics 448, 1–19. https://doi.org/10.1016/j.tecto.2007.11.005.

Le Roux, V., Lee, C.T.A., Turner, S.J., 2010. Zn/Fe systematics in mafic and ultramafic systems: implications for detecting major element heterogeneities in the Earth's mantle. Geochim. Cosmochim. Acta 74, 2779–2796. https://doi.org/10.1016/j.gca.2010.02.004.

Le Roux, V., Dasgupta, R., Lee, C.T.A., 2011. Mineralogical heterogeneities in the Earth's mantle: Constraints from Mn, Co, Ni and Zn partitioning during partial melting. Earth Planet. Sci. Lett. 307, 395–408. https://doi.org/10.1016/j.epsl.2011.05.014.

Lee, C.T.A., Luffi, P., Plank, T., Dalton, H., Leeman, W.P., 2009. Constraints on the depths and temperatures of basaltic magma generation on Earth and other terrestrial planets using new thermobarometers for mafic magmas. Earth Planet. Sci. Lett. 279, 20–33. https://doi.org/10.1016/j.epsl.2008.12.020.

Link, K., Koehn, D., Barth, M.G., Tiberindwa, J.V., Barifaijo, E., Aanyu, K., Foley, S.F., 2010. Continuous cratonic crust between the Congo and Tanzania blocks in western Uganda. Int. J. Earth Sci. 99, 1559–1573. https://doi.org/10.1007/s00531-010-0548-8.

Lloyd, F.E., 1981. Upper-mantle metasomatism beneath a continental rift: clinopyroxenes in alkali mafic lavas and nodules from South West Uganda. Mineral. Mag. 44, 315–323. https://doi.org/10.1180/minmag.1981.044.335.12.

Lloyd, F.E., 1987. Characterization of mantle metasomatic fluids in spinel lherzolites and alkali clinopyroxenites from the West Eifel and South West Uganda. Mantle Metasomatism. Academic Press London, pp. 91–123.

Lloyd, F.E., Arima, M., Edgar, A.D., 1985. Partial melting of a phlogopite-clinopyroxenite nodule from south-west Uganda: an experimental study bearing on the origin of highly potassic continental rift volcanics. Contrib. Mineral. Petrol. 91, 321–329. https://doi.org/10.1007/BF00374688.

Lloyd, F.E., Edgar, A.D., Ragnarsdottir, K.V., 1996. LREE distribution in perovskite, apatite and titanite from South West Ugandan xenoliths and kamafugite lavas. Mineral. Petrol. 57, 205–228. https://doi.org/10.1007/BF01162359.

MacGregor, D., 2015. History of the development of the East African Rift System: A series of interpreted maps through time. Journal of African Earth Sciences 101, 232–252. https://doi.org/10.1016/j.jafrearsci.2014.09.016.

Mana, S., Furman, T., Carr, M.J., Mollel, G.F., Mortlock, R.a., Feigenson, M.D., Turrin, B.D., Swisher, C.C., 2012. Geochronology and geochemistry of the Essimingor volcano: Melting of metasomatized lithospheric mantle beneath the North Tanzanian Divergence zone (East African Rift). Lithos 155, 310–325. https://doi.org/10.1016/j.lithos.2012.09.009.

Min, K., Mundil, R., Renne, P.R., Ludwig, K.R., 2000. A test for systematic errors in 40Ar/39Ar geochronology through comparison with U/Pb analysis of a 1.1-Ga rhyolite. Geochim. Cosmochim. Acta 64, 73–98. https://doi.org/10.1016/S0016-7037(99)00204-5.

Muravyeva, N.S., Senin, V.G., 2016. Glimmerite-Wehrlite xenolith from the Ugandite of East African rift: mineral composition and conditions of formation. Geochem. Int. 54, 457–463. https://doi.org/10.1134/S0016702916050062.

Muravyeva, N.S., Senin, V.G., 2018. Xenoliths from Bunyaruguru volcanic field: some insights into lithology of East African Rift upper mantle. Lithos 296–299, 17–36. https://doi.org/10.1016/j.lithos.2017.10.023.

Muravyeva, N.S., Belyatsky, B.V., Senin, V.G., Ivanov, A.V., 2014. Sr–Nd–Pb isotope systematics and clinopyroxene-host disequilibrium in ultra-potassic magmas from Toro-Ankole and Virunga, East-African Rift: Implications for magma mixing and source heterogeneity. Lithos 210–211, 260–277. https://doi.org/10.1016/j.lithos.2014.09.011.

Neave, D.A., Putirka, K.D., 2017. A new clinopyroxene-liquid barometer, and implications for magma storage pressures under Icelandic rift zones. Am. Mineral. 102, 777–794.

Nelson, W.R., Furman, T., Pitcavage, E., 2015. Exploring the link between metasomatized lithosphere and continental rifting: a case study of the East African Rift System. Geological Society of America Abstracts with Programs. 47, p. 351 7.

Nixon, P.H., 1967. The Geology of Fort Portal and Kasekere Volcanic Fields. Geol. Surv. Uganda Report No.

Paslick, C., Halliday, A., James, D., Dawson, J.B., 1995. Enrichment of the continental lithosphere by OIB melts: evidence from the volcanic province of northern Tanzania. Earth and Planetary Science Letters 130, 109–126.

Pik, R., Deniel, C., Coulon, C., Yirgu, G., Hofmann, C., Ayalew, D., 1998. The northwestern Ethiopian Plateau flood basalts: classification and spatial distribution of magma types. J. Volcanol. Geotherm. Res. 81, 91–111. https://doi.org/10.1016/S0377-0273(97)00073-5.

Pilet, B., Baker, M.B., Muntener, O., Stolper, E.M., 2011. Monte Carlo simulations of metasomatic enrichment in the lithosphere and implications for the source of alkaline basalts. J. Petrol. 52, 1415–1442. https://doi.org/10.1093/petrology/egr007.

Pitcavage, E., 2020. Geochemical Investigations of Continental Rift Magmatism: A Case Study in East Africa's Western Rift. Pennsylvania State University.

Plank, T., 2014. The Chemical Composition of Subducting Sediments. Treatise on Geochemistry: Second Edition 607–629.

Pouclet, A., Bellon, H., Bram, K., 2016. The Cenozoic volcanism in the Kivu rift: Assessment of the tectonic setting, geochemistry, and geochronology of the volcanic activity in the South-Kivu and Virunga regions. J. Afr. Earth Sci. 121, 219–246. https://doi.org/10.1016/j.jafrearsci.2016.05.026.

Putirka, K., Johnson, M., Kinzler, R., Longhi, J., Walker, D., 1996. Thermobarometry of mafic igneous rocks based on clinopyroxene-liquid equilibria, 0–30 kbar. Contrib. Mineral. Petrol. 123, 92–108. https://doi.org/10.1007/s004100050145.

Roberts, E.M., Stevens, N.J., O'Connor, P.M., Dirks, P.H.G.M., Gottfried, M.D., Clyde, W.C., Armstrong, R.A., Kemp, A.I.S., Hemming, S., 2012. Initiation of the western branch of the East African Rift coeval with the eastern branch. Nat. Geosci. 5, 289–294. https://doi.org/10.1038/ngeo1432.

Rogers, N.W., De Mulder, M., Hawkesworth, C.J., 1992. An enriched mantle source for potassic basanites: evidence from Karisimbi volcano, Virunga volcanic province, Rwanda. Contrib. Mineral. Petrol. 111, 543–556.

Rogers, N.W., James, D., Kelley, S.P., De Mulder, M., 1998. The generation of potassic lavas from the Eastern Virunga Province, Rwanda. J. Petrol. 39, 1223–1247. https://doi.org/10.1093/petroj/39.6.1223.

Rooney, T.O., 2017. The Cenozoic magmatism of East-Africa: part I — flood basalts and pulsed magmatism. Lithos 286–287, 264–301. https://doi.org/10.1016/j.lithos.2017.05.014.

Rooney, T.O., Nelson, W.R., Dosso, L., Furman, T., Hanan, B., 2014. The role of continental lithosphere metasomes in the production of HIMU-like magmatism on the northeast African and Arabian plates. Geology 42, 419–422. https://doi.org/10.1130/G35216.1.

Rosenthal, A., Foley, S.F., Pearson, D.G., Nowell, G.M., Tappe, S., 2009. Petrogenesis of strongly alkaline primitive volcanic rocks at the propagating tip of the western branch of the East African Rift. Earth Planet. Sci. Lett. 284, 236–248. https://doi.org/10.1016/j.epsl.2009.04.036.

Rudnick, R.L., McDonough, W.F., Chappell, B.W., 1993. Carbonatite metasomatism in the northern Tanzanian mantle: petrographic and geochemical characteristics. Earth Planet. Sci. Lett. 114, 463–475. https://doi.org/10.1016/0012-821X(93)90076-L.

Sack, R.O., Walker, D., Carmichael, I.S.E., 1987. Experimental petrology of alkalic lavas: constraints on cotectics of multiple saturation in natural basic liquids. Contrib. Mineral. Petrol. 96, 1–23.

Stamps, D.S., Calais, E., Saria, E., Hartnady, C., Nocquet, J.-M., Ebinger, C.J., Fernandes, R.M., 2008. A kinematic model for the East African Rift. Geophys. Res. Lett. 35, L05304. https://doi.org/10.1029/2007GL032781.

Stewart, K., Rogers, N., 1996. Mantle plume and lithosphere contributions to basalts from southern Ethiopia. Earth Planet. Sci. Lett. 139, 195–211. https://doi.org/10.1016/0012-821x(96)00015-5.

Sun, S.-S., McDonough, W.F., 1989. Chemical and isotopic systematics of oceanic basalts: implications for mantle composition and processes. Geol. Soc. London Spec. Publ. 42, 313–345.

Tappe, S., Romer, R.L., Stracke, A., Steenfelt, A., Smart, K.A., Muehlenbachs, K., Torsvik, T.H., 2017. Sources and mobility of carbonate melts beneath cratons, with implications for deep carbon cycling, metasomatism and rift initiation. Earth Planet. Sci. Lett. 466, 152–167. https://doi.org/10.1016/j.epsl.2017.03.011.

Vollmer, R., Norry, M., 1983. Possible origin of K-rich volcanic rocks from Virunga, East Africa, by metasomatism of continental crustal material: Pb, Nd and Sr isotopic evidence. Earth Planet. Sci. Lett. 64, 374–386.

Wang, K., Plank, T., Walker, J.D., Smith, E.I., 2002. A mantle melting profile across the Basin and Range, SW USA. J. Geophys. Res. 107.

Wessel, P., Luis, J.F., Uieda, L., Scharroo, R., Wobbe, F., Smith, W.H.F., Tian, D., 2019. The Generic Mapping Tools Version 6. Geochemistry, Geophysics, Geosystems 20, 5556–5564. https://doi.org/10.1029/2019GC008515.

Wölbern, I., Rümpker, G., Schumann, A., Muwanga, A., 2010. Crustal thinning beneath the Rwenzori region, Albertine rift, Uganda, from receiver-function analysis. Int. J. Earth Sci. 99, 1545–1557. https://doi.org/10.1007/s00531-009-0509-2.

Woolley, A.R., Church, A.A., 2005. Extrusive carbonatites: a brief review. Lithos 85, 1–14. https://doi.org/10.1016/j.lithos.2005.03.018.